

Research Articles | Neurobiology of Disease

Hippocampal neural stem cell exosomes promote brain resilience against the impact of tau oligomers.

<https://doi.org/10.1523/JNEUROSCI.1664-24.2025>

Received: 27 September 2024

Revised: 20 December 2024

Accepted: 28 January 2025

Copyright © 2025 the authors

This Early Release article has been peer reviewed and accepted, but has not been through the composition and copyediting processes. The final version may differ slightly in style or formatting and will contain links to any extended data.

Alerts: Sign up at www.jneurosci.org/alerts to receive customized email alerts when the fully formatted version of this article is published.

1 **Title: Hippocampal neural stem cell exosomes promote brain resilience against**
2 **the impact of tau oligomers.**

3 **Abbreviated title:** Brain resilience against tau oligomers

4 Balaji Krishnan², Michela Marcatti², Anna Fracassi², Wen-Ru Zhang², Jutatip Guptarak²,
5 Kathia Johnson¹, Auston Grant¹, Rakez Kayed², Giulio Tagliatela^{2†}, Maria-Adelaide
6 Micci^{1†}.

7 †These authors contributed equally to this work.

8 Author affiliations:

9 1 Department of Anesthesiology, University of Texas Medical Branch, Galveston, TX
10 77555

11 2 Mitchell Center for Neurodegenerative Diseases, Department of Neurology, University
12 of Texas Medical Branch, Galveston, TX 77555

13
14 Balaji Krishnan: bakrishn@utmb.edu; Michela Marcatti: mimarcatt@utmb.edu; Wen-Ru
15 Zhang: wezhang@utmb.edu; Anna Fracassi: anfracas@utmb.edu; Jutatip Guptarak:
16 juguptat@utmb.edu; Kathia Johnson: kevjjhon@utmb.edu; Auston Grant:
17 acgrant@utmb.edu; Rakez Kayed: rakayed@utmb.edu; Giulio Tagliatela:
18 gtaglial@utmb.edu; Maria-Adelaide Micci: mmicci@utmb.edu.

19 **Correspondence to:** Maria-Adelaide Micci, Department of Anesthesiology, University
20 of Texas Medical Branch, Galveston, TX 77555. E-mail: mmicci@utmb.edu; Giulio
21 Tagliatela, Mitchell Center for Neurodegenerative Diseases, Department of Neurology,
22 University of Texas Medical Branch, Galveston, TX 77555. E-mail: gtaglial@utmb.edu;

23

24

25 **Number of Pages:**

26

27 **Number of Figures:**

28

29 **Number of Tables:**

30

31 **Number of Words:**

32

33 **Abstract: 231**

34

35 **Introduction: 576**

36

37 **Discussion: 1173**

38

39

40

41 **Conflict of Interest Statement:** The authors declare no competing financial interests

42

43 **Acknowledgements:** We thank Dr. Vsevolod L. Popov and Ms. Zhixia Ding for helpful
44 suggestions and for the use of the Department of Pathology EM facility, and Stacy L. Sell, PhD,
45 for editing.

46

47 **Abstract**

48 A promising therapeutic intervention for preventing the onset and progression of
49 Alzheimer's Disease (AD) is to protect and improve synaptic resilience, a well-established
50 early vulnerability associated with the toxic effects of oligomers of Ab (AbO) and Tau
51 (TauO). We have previously reported that exosomes from hippocampal neural stem cells
52 (NSCs) protect synapses against A β O. Here, we demonstrate how exosomes can also
53 shield against TauO toxicity in adult mice synapses, potentially benefiting primary and
54 secondary tauopathies. Exosomes from hippocampal NSCs (NSCexo) or mature neurons
55 (MNexo) were delivered intracerebroventricularly to adult wildtype male mice (C57Bl6/J).
56 After 24 hours, TauO were administered to suppress long-term potentiation (LTP) and
57 memory, measured by electrophysiology and contextual memory deficits measured using
58 novel object recognition (NOR) test. We also assessed TauO binding to synapses using
59 isolated synaptosomes and cultured hippocampal neurons. Furthermore, mimics of select
60 miRNAs present in NSCexo, were delivered ICV to mice prior to assessment of TauO-
61 induced suppression of hippocampal LTP. Our results showed that NSC-, not MN-,
62 derived exosomes, prevented TauO-induced memory impairment, LTP suppression, and
63 reduced Tau accumulation and TauO internalization in synaptosomes. These findings
64 suggest that NSC-derived exosomes can protect against synaptic dysfunction and
65 memory deficits induced by both A β O and TauO, offering a novel therapeutic strategy for
66 multiple neurodegenerative states.

67 **Significance Statement:** NSCexo provide an unprecedented therapeutic strategy
68 targeting an early vulnerability driven by amyloidogenic toxic oligomers associated with
69 multiple neurodegenerative states.

70 **Keywords:** Alzheimer's Disease; Tau oligomers; miRNAs, Neural Stem Cells;
71 Exosomes; Synapses

72

73 **Introduction**

74 Alzheimer's disease (AD) stands as the most prevalent form of age-related
75 neurodegenerative dementia in the United States, with projections indicating that the
76 number of affected individuals will more than double by 2050. Despite ongoing efforts,
77 effective treatments for AD remain elusive, prompting a consensus that successful
78 therapies should target prevention and/or minimization of symptoms prior to the onset of
79 irreversible neuronal loss that characterizes the disease's advanced stages
80 (<https://www.alz.org/media/documents/alzheimers-facts-and-figures.pdf>).

81 Over the last two decades, AD research has been significantly shaped by the
82 identification of individuals who maintained cognitive function despite advanced AD
83 pathology, termed Non-Demented with AD Neuropathology (NDAN). (Zolochovska and
84 Tagliavola, 2016) This discovery highlights the brain's potential to resist or delay the
85 neurotoxic processes that typically lead to cognitive decline in AD. Notably, our previous
86 research uncovered distinctive proteomic profiles in hippocampal synapses of NDAN
87 subjects, (Zolochovska et al., 2018) along with resistance to harmful amyloid β oligomers
88 (A β O). (Bjorklund et al., 2012) As synaptic dysfunction, induced by A β O and tau oligomers
89 (TauO), emerges as an early event in AD progression, (Klein, 2013; Spiess-Jones and
90 Hyman, 2014; Tu et al., 2014; Fa et al., 2016; Selkoe and Hardy, 2016) preserving
91 synaptic integrity, as observed in NDAN individuals, holds promise as a therapeutic
92 approach, albeit challenging to achieve.

93 New neurons are generated from neural stem cells (NSCs) via a process known as
94 neurogenesis. (Altman and Das, 1965) Neurogenesis occurs in the mammalian brain, in
95 the hippocampus, throughout life and is known to contribute to brain plasticity and
96 repair. (Altman and Das, 1965) Extensive evidence indicates that hippocampal
97 neurogenesis decreases significantly more in individuals with AD than in those
98 experiencing normal aging. (Kuhn et al., 2007; Mu and Gage, 2011; Hamilton et al., 2013;
99 Horgusluoglu et al., 2017); (deToledo-Morrell et al., 2007; Ohm, 2007; Appel et al., 2009;
100 Barnes et al., 2009) Our research revealed that the brains of NDAN individuals exhibit
101 greater numbers of hippocampal NSCs compared to the brains of healthy age-matched

102 controls.(Briley et al., 2016) This suggests that maintaining robust neurogenesis could
103 mitigate cognitive decline in the presence of AD pathology.

104 Neural stem cells release exosomes,(Marzesco et al., 2005; Stevanato et al., 2016) small
105 vesicles containing various molecular components, including microRNAs
106 (miRNAs),(Raposo and Stoorvogel, 2013; Sato-Kuwabara et al., 2015) which are
107 increasingly recognized for their role in mediating the functional effects of NSCs.(Baulch
108 et al., 2016; Han et al., 2016; Zhang et al., 2017) These exosomes have been implicated
109 in controlling aging processes(Zhang et al., 2017) and ameliorating synaptic dysfunction
110 and cognitive decline in AD models.(Cui et al., 2018) Moreover, a meta-analysis reveals
111 a connection between exosomes, synaptic plasticity, and neurodegenerative diseases,
112 including AD.(Wang et al., 2017)

113 Our previous research indicated that hippocampal NSC-derived exosomes rendered
114 central nervous system (CNS) synapses resistant to A β O by delivering specific miRNA
115 cargo.(Micci et al., 2019) Additionally, we found that compared to individuals with AD, the
116 brains of NDAN subjects exhibited increased numbers of NSCs in the hippocampus.
117 Since the number of NSCs, but not neurons, positively correlated with cognitive function,
118 we hypothesized that NSCs may support cognitive resilience through mechanisms other
119 than neurogenesis.(Briley et al., 2016)

120 Building on these findings, here we investigate whether NSC-secreted exosomes
121 (NSCexo) prevent functional synaptic deficits and memory impairments driven by TauO
122 and whether this protection involves enhanced synaptic resistance to TauO binding.
123 Moreover, given that miRNAs are a predominant cargo of exosomes, we aimed to identify
124 specific miRNAs found exclusively or highly enriched in exosomes derived from NSCs
125 that may mediate their protective effects on target neuronal synapses.

126

127

128 **Materials and methods**

129

130 **Animals**

131 Male mice (C57BL/6J; 6-8 weeks old) were purchased from Jackson Laboratories (Bar
132 Harbor, ME). The Institutional Animal Care and Use Committee of the University of Texas
133 Medical Branch, Galveston, Texas, approved all animal experiments, which were
134 conducted according to the National Institutes of Health Guide for the Care and Use of
135 Laboratory Animals. The mice were housed four per cage on a 12/12/light dark cycle with
136 free access to food and water.

137 **Randomization and blinding procedures**

138 Animals were randomized to the experimental groups using a simple randomization
139 procedure. To maximize scientific rigor, a simple blinding procedure was achieved by
140 coding exosome preparations (NSC-exo or MN-exo), vehicle, or the miRNAs to be
141 employed in the various experiments. The correspondence of the codes was known only
142 to Guilio Tagliatela, PhD and Maria-Adelaide Micci, PhD and was revealed only after
143 final statistical analyses were performed.

144 **Neural stem cell (NSC) and mature neuron (MN) cultures**

145 Adult rat hippocampal NSCs were purchased from MilliporeSigma (Temecula, CA). NSCs
146 were cultured as neurospheres on low-attachment plates in expansion media consisting
147 of: EmbryoMax DMEM/F12 containing L-Glutamine without HEPES, B27-with retinoic
148 acid, GlutaMAX™ (all from Gibco, ThermoFisher Scientific, Waltham, MA), FGF-b (20
149 ng/ml, MilliporeSigma, Temecula, CA) and antibiotics (PSF, Gibco, ThermoFisher
150 Scientific, Waltham, MA). Cells were passaged every five to seven days using
151 Neuropapain (Genlantis, San Diego, CA).

152 For the generation of mature neurons (MN), NSC neurospheres were dissociated using
153 Neuropapain (Genlantis, San Diego, CA), 2 mg/ml in basal media, plated out onto poly-
154 ornithine/laminin-coated plates at a density of 8.0×10^5 cells/cm² and cultured in
155 differentiation media consisting of expansion media without FGFb and with the addition
156 of 1 μ M retinoic acid (MilliporeSigma, Temecula, CA) and five μ M forskolin

157 (MilliporeSigma, Temecula, CA) for five days. Immunocytochemistry and western blot
158 analyses confirmed the purity of the cultures by identifying the presence or absence of
159 specific NSCs (Sox2 and nestin) and neuronal markers (βIII-tubulin and NeuN) as
160 previously reported .(Micci et al., 2019)

161 **Tau oligomers preparation**

162 Prepared recombinant TauO were provided by Rakez Kayed, PhD's laboratory. They
163 were produced and characterized following established and published protocols,(Gerson
164 et al., 2017; Sengupta et al., 2018) and labeled TauO488 using the Microscale Protein
165 Labeling Kit from ThermoFisher (cat# A30006; lot# 2413458) following the manufacturer's
166 instructions. Briefly, 100 µl of TauO 1 mg/ml was mixed with 1/10 volume of 1M sodium
167 bicarbonate. Then, 11.3 µl of the Alexa Fluoro 488 TFP ester was added following the kit
168 molar ratio recommendations and incubated for 15 m at room temperature. The labeled
169 TauO were purified by centrifugation at 16000 x g in spin filters with yields between 60
170 and 90% and quantified spectrophotometrically using a Nanodrop 2000C (ThermoFisher)
171 to be used for flow cytometry analyses. The determined degree of labeling (DOL) was
172 higher than two.

173 **Isolation and characterization of exosomes**

174 Exosomes were isolated from conditioned culture media using the ultracentrifugation
175 method.(Greening et al., 2015; Lobb et al., 2015) Comprehensive characterization of
176 isolated exosomes was performed using electron microscopy (EM), dot blotting, and
177 nanoparticle tracking analyses (Figure 1) according to the guidelines of the International
178 Society of Extracellular Vesicles(Lotvall et al., 2014; Witwer et al., 2021) and as previously
179 reported.(Micci et al., 2019) Briefly, 225 ml of conditioned media collected from
180 approximately 60 million cultured cells (NSC or mature neurons) were centrifuged at
181 2,000 x g, at 4°C for 10 minutes to remove cells and debris. The resulting supernatant
182 was transferred to new tubes and centrifuged at 10,000 x g, at 4 °C for 10 minutes. The
183 supernatant was transferred to Beckman 60 Ti ultracentrifuge tubes and centrifuged at
184 100000 x g for three hours at 4°C. The resulting pellet was resuspended in 2 ml PBS
185 containing a protease inhibitor cocktail (MilliporeSigma, Temecula, CA), and centrifuged
186 at 182,000 x g for one hour at 4°C in a Beckman TLA110 centrifuge. The resulting pellet,

187 containing exosomes, was resuspended in 1X PBS containing protease inhibitors to a
188 concentration of approximately 10^9 exosomes per microliter.

189 Ultrastructure analysis of exosomes was performed with 5 μ l drops adsorbed on a 200-
190 mesh coated resin grid (FCF 200 – CU Formvar/Carbon, Electron Microscopy Sciences,
191 Hatfield, PA, USA) for 10 min at room temperature (RT). Grids were blotted with filter
192 paper and stained with 2% aqueous uranyl acetate (cat# 541-09-3, Electron Microscopy
193 Sciences) for negative staining for 1 min at RT. The uranyl acetate was then removed
194 using filter paper, and the grids were dried with warm regular light for 2 min. Images were
195 acquired with a Philips CM-100 transmission electron microscope at 60 kV with an Orius
196 SC2001 digital camera (Gatan, Pleasanton, CA, USA). For dot blot NSCexo, MNexo, and
197 mouse parietal cortex were lysed with RIPA buffer containing protease inhibitors and 0.5
198 μ g of each sample was dotted on a S nitrocellulose membrane. The membrane was let
199 dry at room temperature (RT) for 30 minutes, blocked with Intercept® (TBS) Blocking
200 Buffer (LI-COR Bioscience) for 1 hour at RT, and probed overnight at 4 °C with primary
201 antibodies against CD9, CD63, CD81, Hsp70 and GM130 (1:1000; EXOABSBI
202 Biotechnology), followed by IR Dye® secondary antibodies (1:1000; LI-COR
203 Biosciences). Nanoparticle tracking analysis was performed using the NanoSight N300
204 system and NTA 2.1 operating system (Malvern) according to manufacturer's instructions.
205 Briefly, the exosome preparation was diluted in PBS and injected into the NanoSight for
206 analysis of both particle size and concentration.

207 **Intracerebroventricular injections**

208 Adult (six to eight week-old) male C57BL/6J mice were anesthetized with isoflurane and
209 subjected to ICV injections using the freehand injection method.(Clark et al., 1968;
210 Dineley et al., 2010; Krishnan et al., 2018). One day after ICV injection of exosomes
211 (prepared from NSC or MN conditioned media) or PBS (vehicle), mice were euthanized
212 for the electrophysiology study or injected ICV with 3ml of 0.55mM TauO (prepared as
213 described above) or ACSF and euthanized 24 h later (for biochemistry studies) or 48 h
214 later (after behavioral testing) by deep usoflurane anesthesia followed by decapitation.
215 Brains were removed and divided into two groups: 1) fresh hippocampal slices were
216 prepared for assessment of LTP or 2) brains were further dissected into hippocampus,

217 frontal cortex, parieto-occipital cortex, and midbrain, snap frozen on dry ice, and stored
218 at -80 °C until ready to use for the synaptosome preparation.

219 **Brain slice preparation and electrophysiological assessment of long-term** 220 **potentiation (LTP)**

221 Brain slices were prepared and electrophysiological assessment of LTP was performed
222 according to the methods reported by Ting *et al.* (Ting *et al.*, 2014) Mice were deeply
223 anesthetized with isoflurane and transcardially perfused with 25-30 mL of room
224 temperature carbogenated gas mixture (95% O₂ and 5% CO₂) and NMDG ACSF
225 consisting of 93 mM NMDG, 2.5 mM KCl, 1.25 mM NaH₂PO₄, 30 mM NaHCO₃, 20 mM
226 HEPES, 25 mM glucose, 2 mM thiourea, 5 mM Na-ascorbate, 3 mM Na-pyruvate, 0.5 mM
227 CaCl₂·2H₂O, and 10 mM MgSO₄·7H₂O, titrated to pH 7.3–7.4 with HCl.

228 Following perfusion, brains were carefully extracted within 1 min. Each brain was
229 mounted using Super Glue[®], on the mounting cylinder, at a transverse slicing angle, to
230 generate 350 μm sections using the Compresstome VF-300 (Precisionary Instruments)
231 protocols. The sliced hippocampi were allowed to recover from the procedure at 32-34 °C
232 for <12 min. The slices were then transferred to a new holding chamber with carbogen-
233 saturated HEPES ACSF recovery solution (92 mM NaCl, 2.5 mM KCl, 1.2 mM NaH₂PO₄,
234 30 mM NaHCO₃, 20 mM HEPES, 25 mM glucose, 2 mM thiourea, 5 mM Na-ascorbate, 3
235 mM Na-pyruvate, 2 mM CaCl₂·2H₂O and 2 mM MgSO₄·7H₂O) at pH 7.3-7.4, RT.

236 Recording was done in constantly flowing oxygenated (95% O₂/5% CO₂) ice-cold normal
237 ACSF consisting of (in mM) 124 NaCl, 2.5 KCl, 1.2- NaHPO₄, 24 NaHCO₃, 5 HEPES, 13
238 Glucose, 2 CaCl₂·2H₂O, 1.2 Mg SO₄·7H₂O, at pH 7.3-7.4. Slices were perfused at a rate
239 of approximately three mL/min. Field excitatory post-synaptic potentials (fEPSPs) were
240 collected using an Axon MultiClamp 700B amplifier connected to a Windows computer
241 running Clampex 8.2 software (Molecular Devices). All electrodes were placed under the
242 visual guidance of an upright microscope (Olympus BX51WI). The slope from a single
243 fEPSP trace was calculated from the initial slope of the fEPSP relative to the slope of the
244 10 ms interval immediately preceding afferent stimulation. The current magnitude was
245 delivered through a digital stimulus isolation amplifier (AMPI, ISRAEL) and set to elicit a
246 fEPSP of approximately 30% of maximum for synaptic potentiation experiments using

247 platinum-iridium tipped concentric bipolar electrodes (SUK 30200, FHC Inc, Bowdoin,
248 ME). Using a horizontal P-97 Flaming/Brown Micropipette puller (Sutter Instruments),
249 borosilicate glass capillaries (catalog# BF150-110-10, Sutter Instruments, Novato, CA)
250 were used to pull electrodes and filled with ACSF to get a resistance of 1–2 MΩ.

251 A stable baseline (for a minimum of 10 m) was obtained by delivering a single pulse
252 stimulation at 20 s interstimulus intervals. Field excitatory post-synaptic potentials in the
253 CA1 were evoked by stimulating the Schaffer collaterals (SC: CA3->CA1) using a
254 conditioning stimulus (CS) consisting of three trains of 100 pulses at 100 Hz, 20 s apart
255 (high-frequency stimulation; HFS). Input-output experiments were conducted to measure
256 basal dendritic excitation in response to increasing applied current in ACSF. Evoked
257 fEPSP responses were digitized via Digidata 1550B, and the initial slope of the fEPSP
258 was analyzed using pClamp 10.6 software (Molecular Devices). All data are represented
259 as percentage change from the initial average fEPSP slope, defined as the average slope
260 obtained for the 10 m prior to CS application.

261 **Intracerebroventricular injection technique**

262 Intracerebroventricular (ICV) injections were performed on deeply anesthetized mice
263 using a 29-gauge needle, firmly held in place using hemostatic forceps to leave 4.5 mm
264 of the needle tip exposed and connected to a 25 µl Hamilton syringe via 0.38 mm
265 polyethylene tubing. Infusions were performed at the rate of 2 µl/min for a total volume of
266 3 ml, using an electronic programmable microinfuser (Harvard Apparatus). After ICV
267 injection, the needle was left in place for 2 min, and the mouse was allowed to recover
268 while lying on a heated pad under warm light.

269 **Novel Object Recognition testing**

270 The Novel Object Recognition test (NOR) was performed as described
271 previously.(Tagliatela et al., 2009; Comerota et al., 2017; Krishnan et al., 2018) Each
272 mouse was habituated to an empty NOR open field box that served to test each animal
273 for normal locomotion. The sessions commenced with two 10 m habituation sessions
274 spaced 24 h apart, during which the TopScan (Clever Sys. Inc., Reston, VA) video-
275 tracking software quantified various locomotor parameters. Twenty-four hours after the
276 last habituation session, mice were subjected to 10 m training sessions consisting of

277 exposure to two identical, non-toxic objects (metal or hard plastic items) in the same open
278 field box to which the mouse had previously been acclimated, so that the mice would be
279 more likely to maximize time exploring the objects as opposed to the environment.

280 The time spent exploring each object was recorded using ObjectScan (Clever Sys. Inc.).
281 Time spent in each quadrant zone, and object zone surrounding each object, was also
282 recorded. After the training session, the animal was returned to its home cage. Mice were
283 returned once more to the same box after retention intervals of either two or 24 h, for the
284 test session. In the box would be one object identical to the familiar one but previously
285 unused (to prevent olfactory cues) and one completely unfamiliar, hence, novel, object.
286 The animal was allowed to explore for 10 m, during which the amount of time spent
287 exploring each object was recorded.

288 Objects were randomized and counterbalanced across animals. The ratio of the time
289 spent exploring the novel object versus the time spent exploring the familiar object was
290 reported as the Discrimination Index. (Buenz et al., 2009; Bussian et al., 2018) An index
291 above 1 is indicative of recognition that an object is novel. Each mouse was tested at 2-
292 and 24-hour intervals, with the intention of assessing the shorter and longer time frames
293 in memory recall. To avoid the experience in the 2-hour test affecting the performance in
294 the 24-hour test, different novel objects were used for the two memory recall tests.

295 **Tissue collection and processing**

296 Animals were deeply anesthetized using isoflurane and transcardially perfused with PBS. Brains
297 were carefully removed and then cut in two halves along the sagittal line. One hemisphere was
298 collected for biochemistry assays. The other hemisphere was post-fixed in 4% paraformaldehyde
299 in 0.1 M PBS, pH 7.4 for 48 hr at 4°C, and cryoprotected by suspension in 30% sucrose solution
300 for 48 h at 4°C. Brains were then embedded in OCT compound (Tissue-Tek, Tokyo, Japan) and
301 frozen on dry ice prior to storage at -80°C. For immunofluorescence experiments, mouse brain
302 blocks were removed from storage at -80°C, equilibrated at -20°C and sectioned at 12 µm onto
303 Superfrost/Plus slides (catalog# 12-550-15, Fisherbrand, ThermoFisher Scientific, Waltham, MA,
304 USA). Prepared slides were stored at -80°C.

305 **Immunofluorescence staining**

306 Slides were processed as previously described.(Fracassi et al., 2023) Briefly, slides were
307 fixed in 4% paraformaldehyde in 0.1 M PBS, pH 7.4, for 30 m at RT. Nonspecific binding
308 sites were blocked with 5% bovine serum albumin (BSA) (catalog# A4503-100G, Sigma-
309 Aldrich Inc., Saint Louis, MO, USA)/10% normal goat serum (NGS, catalog# S26-100ml
310 Sigma-Aldrich) and sections were permeabilized with 0.5% Triton X-100/0.05% Tween-
311 20 for 1h at RT. Slides were incubated overnight at 4°C with the following primary
312 antibodies diluted in PBS containing 1.5% NGS: chicken anti-Tau (1:100, #ab75714,
313 Abcam – Cambridge Science Park, Cambridge, UK); mouse anti-phospho-Tau
314 (Ser202/Thr205 - AT8) (1:100, MN1020, ThermoFisher); rabbit anti-NeuN (1:200,
315 #12943S Cell Signaling Technology, Inc., Danvers, MA, USA). Slides were washed in
316 PBS before incubation with the appropriate Alexa-conjugated secondary antibodies (goat
317 anti-chicken Alexa Fluor 594, 1:400, # A-11042; goat anti-mouse Alexa Fluor 488, #A-
318 10680, goat anti-rabbit Alexa Fluor 647, 1:400, #A32733, ThermoFisher Scientific) in PBS
319 containing 1.5% NGS/0.25% Triton X-100 for one hr at RT. Finally, slides were washed
320 in PBS, treated with 0.3% Sudan Black B prepared in 70% EtOH for 10 m to block
321 lipofuscin autofluorescence, washed again with deionized water, and coverslipped using
322 Fluoromount-G containing 4',6-diamidino-2-phenylindole (DAPI) (Cat# 0100-20,
323 SouthernBiotech, Birmingham, AL, USA) and sealed.

324 **Quantitative analysis of immunofluorescence**

325 All immunoreacted sections were acquired with a Keyence BZ-X800 (Keyence Corporation,
326 Osaka, Japan) microscope by using immersion oil 60X. Three sections were analyzed for each
327 animal, and at least two images per section were taken at 1,920 × 1,440-pixel resolution, with the
328 z-step size of 2 μm at 12 μm thickness. We analyzed five different regions: dentate gyrus (DG),
329 CA1, CA3, frontal and parietal cortex. For the feasibility of the quantification, all layers from a
330 single image stack were projected on a single slice (stack/Z projection). Quantitative analyses
331 were performed using ImageJ software (<https://imagej.nih.gov/ij>, NIH, Bethesda, MD, USA). We
332 analyzed the intensity of fluorescence for each marker (Tau and posphoTau AT8) *per area*
333 (Integrated Density, IntDen) when the overall distribution of a specific marker was studied. The
334 colocalization between Tau and either NeuN or Iba1 was evaluated and quantified using
335 Pearson's correlation coefficient (PCC). Representative images were composed in an Adobe
336 Photoshop CC2020 format.

337 **Synaptosome isolation**

338 We isolated synaptosomes from the hippocampi of mice previously injected ICV with
339 PBS, NSCexo, or MNexo. The synaptosomal fraction containing both pre- and post-
340 synaptic components was isolated using a well-established method developed in our
341 laboratory.(Franklin and Tagliatela, 2016; Comerota et al., 2017; Franklin et al., 2019;
342 Marcatti et al., 2022) Snap frozen hippocampus from mouse brains was lysed using
343 SynPER lysis buffer (Thermo Fisher Scientific, Waltham, MA, USA) with 1% protease and
344 phosphatase cocktail inhibitors, and the homogenates were centrifuged at $1200 \times g$ for
345 10 min at 4°C . The supernatants (containing the synaptosomes) were collected and
346 centrifuged at $15,000 \times g$ for 20 min at 4°C . The synaptosomal pellets were resuspended
347 in HEPES-buffered Krebs-like (HBK) buffer (143.3 mM NaCl, 4.75 mM KCl, 1.2 mM
348 $\text{MgSO}_4 \cdot 7 \text{H}_2\text{O}$, 1.2 mM CaCl_2 , 20.1 mM HEPES, 0.1 mM NaH_2PO_4 , and 10.3 mM D-
349 glucose, pH 7.4). Finally, 0.5% of Pluronic F-68 non-ionic surfactant (cat# 24040-032, lot#
350 2275337; Thermo Fisher Scientific) was added to prevent synaptosome aggregation.

351 The quality and concentration (synaptosomes/ μl) of isolated synaptosomes was routinely
352 verified by flow cytometry, electron microscopy and Western blot as previously
353 reported(Franklin and Tagliatela, 2016; Micci et al., 2019; Marcatti et al., 2022).

354 **Enzyme-linked immunosorbent assay of total Tau**

355 Synaptosomes isolated from the hippocampi of mice injected with PBS, NSCexo, or
356 MNexo (ICV) were challenged with TauO (5 nM) and then digested with proteinase K
357 (PK). Total tau content was measured by commercial Tau enzyme-linked immunosorbent
358 assay (ELISA) kits according to the manufacturer's instructions (cat# KHB0041; Thermo
359 Fisher Scientific, Waltham, MA, USA). Ten million synaptosomes were incubated for 1h
360 at RT with 5 nM of TauO. Half of synaptosomes were incubated with 1 mg/ml of PK (cat#
361 70663-4, lot# 3018798; EMD Millipore) for 30 min at 37°C (1 mg of PK is the equivalent
362 of 30 mAU, where AU is an Anson unit that represents the amount of enzyme that
363 liberates $1.0 \mu\text{mol}$ (181 μg) of tyrosine from casein per min at pH 7.5 at 37°C). The other
364 half was subjected to the same conditions to serve as control. Synaptosomes were then
365 washed three times with HBK buffer, and lysate in 10 μl of Cell Extraction Buffer (cat#
366 FNN0011; Thermo Fisher Scientific, Waltham, MA, USA) containing 0.3M of PMSF and

367 1% protease cocktail inhibitors. Finally, standards and samples were applied to the ELISA
368 plate. After washing, a biotin-conjugated detection antibody was applied. The positive
369 reaction was enhanced with streptavidin–horseradish peroxidase and colored by 3,3',5,5'-
370 tetramethylbenzidine. The absorbance at 450 nm was then measured, and the
371 concentration of tau protein was calculated from the standard curve.

372 **TauO binding challenge to synaptosomes and proteinase K digestion.**

373 Synaptosomes were treated with TauO for binding challenges, and the binding
374 percentages and fluorescence intensity (MFI) were evaluated with flow cytometry. The
375 same number of synaptosomes isolated from each mouse of the three experimental
376 groups was pooled together. We incubated two million synaptosomes for 1 h at RT without
377 oligomers (control) as well as with TauO tagged as described above at concentrations of
378 0, 0.025, 0.05, 0.25, 0.5, 1 μ M. Following the challenge experiments, synaptosomes were
379 digested with 1 mg/ml of PK (cat# 70663-4, lot# 3018798; EMD Millipore) for 30 m at 37
380 $^{\circ}$ C (1 mg of PK is the equivalent of 30 mAU, where AU is an Anson unit that represents
381 the amount of enzyme that liberates 1.0 μ mol (181 μ g) of tyrosine from casein per m at
382 pH 7.5 and 37 $^{\circ}$ C). Synaptosomes were then pelleted, washed three times with HBK
383 buffer, and resuspended in HBK. Oligomer fluorescence positivity was acquired by a
384 Guava EasyCyte 8 flow cytometer (EMD Millipore) and analyzed using Incyte software
385 (EMD Millipore).

386 **Tau oligomer binding to hippocampal neurons *in vitro***

387 Hippocampal neurons were prepared by differentiating adult hippocampal NSC as
388 described above and plated on poly-ornithine/laminin-coated plates. Cultures were
389 treated with exosomes (NSCexo or MNexo; 1×10^6) or an equivalent volume of PBS for
390 24 h at 37 $^{\circ}$ C. After washing, cultures were exposed to 2.5 mM TauO for 60 m at 37 $^{\circ}$ C.
391 One separate set of cells was treated with PBS for 24 h, followed by a vehicle to control
392 for non-specific staining of the anti-hTau antibody. At the end of incubation, the cells were
393 washed and fixed in 4% paraformaldehyde for 15 m. After two washes in PBS, the cells
394 were blocked and permeabilized in PBS containing 5% normal goat serum for 30 m at
395 room temperature. The cells were incubated with mouse anti- β -tubulin primary antibody
396 (1:1000, Promega, Madison, WI) and Tau5 antibody (1:100, ThermoFisher Scientific,

397 Waltham, MA), diluted in 1.5% normal goat serum in PBS overnight at 4°C in a humid
398 chamber. Following three washes in PBS, the cells were incubated with Alexa 488-
399 conjugated anti-mouse and Alexa 594-conjugated anti-rabbit secondary antibodies
400 (1:400; Invitrogen, Carlsbad, CA) in 1.5% normal goat serum in PBS for 1 h at room
401 temperature in a humidified chamber. The cells were washed in PBS and coverslipped
402 with Prolong® Gold AntiFade Reagent with DAPI (ThermoFisher Scientific, Waltham,
403 MA). Images were acquired with an Olympus confocal microscope (FV1200, Olympus
404 Life Science), and quantification of TauO was performed by an investigator blinded to the
405 experimental groups by counting the number of fluorescent puncta in dendrites using
406 ImageJ software.

407 **Intracerebroventricular injection of miRNA mimics and target engagement** 408 **validation**

409 Mice were injected (ICV) with miRNA mimics (scrambled, miR-17, miR-322, miR-485)
410 (ThermoFisher Scientific, Waltham, MA) dissolved in ACSF. Scrambled miRNA was
411 delivered at one nmole per mouse, while 0.33 nmole of miR-17, miR-322, miR-485 were
412 mixed, and a final concentration of one nmole of miRNA per mouse was administered.
413 Four animals per group were used. Twenty-four hours after ICV injection, RNA was
414 extracted from the hippocampi of ICV injected mice using the RNeasy Mini Kit (Qiagen,
415 Venlo, Netherlands), and cDNA was generated with the amfiRivert cDNA Synthesis kit
416 (GenDEPOT, Barker, TX). Quantitative RT-qPCR was performed using specific sense
417 and antisense primers for known targets (STAT3, SYN5X, HIFa3) in a 20ml reaction
418 volume containing 10ml of KAPA SYBR FAST qPCR Master mix (Kapa Biosystems), 0.5
419 ml of 10 µmol/L primer stock, 1 ml cDNA, and 8ml double-distilled H₂O. Data were
420 normalized to b-actin.

421 **Statistical Analysis**

422 The sample sizes were based on a two-sided power analysis performed on the
423 experimental groups to allow us to detect a 10-unit difference in the most variable
424 measurement at $\alpha=0.05$ and $\beta=0.8$ based on the typical variance we have in our data.
425 Data is expressed as mean+/- SEM or SD. Analysis of variance (ANOVA) followed by
426 multiple comparisons post-hoc tests were performed using GraphPad Prism software.

427 Behavioral data (NOR) was analyzed using repeated two-way ANOVA with Dunnett
428 correction for multiple comparisons correction). Immunofluorescence data was analyzed
429 using ordinary one-way ANOVA with Tukey's post hoc test and two-way ANOVA with
430 Šídák's multiple comparisons tests or Tukey's multiple comparisons test where
431 appropriate. For all statistical analyses, significance was defined at $*P<0.05$.

432

JNeurosci Accepted Manuscript

433 **Results**

434 **Neural stem cell-exosomes prevent Tau oligomer-induced short-term memory**
435 **deficits.**

436 Wild-type mice were injected (ICV) with ACSF, NSCexo or MNexo (1×10^9 exosomes)
437 24 h prior to receiving ICV injections of 3 mL of 0.55mM TauO or PBS. The mice
438 underwent NOR training 4 h after treatment, followed by memory recall tests at 2h and
439 24h after that. The treatment schematic is shown in Fig. 2A. Throughout the training
440 phase, animals across all groups exhibited equal exploration of the two identical objects,
441 suggesting that the different treatments had no discernible impact on their inherent
442 exploratory tendencies (Fig. 2B).

443 The ICV injection of ACSF, NSCexo or MNexo alone, akin to the PBS treatment,
444 demonstrated no influence on the mice's capability to differentiate between the familiar
445 and novel object after the 2 h and 24 h testing intervals (Fig. 2C). However, mice
446 administered ACSF or MNexo, followed by ICV injection of TauO, exhibited equivalent
447 exploration time for both the familiar and novel objects during the 2 h memory recall test,
448 indicating memory impairment. On the other hand, mice treated with NSCexo prior to
449 receiving TauO spent significantly more time in the novel object area, revealing preserved
450 memory function despite the administration of the toxic TauO. During the memory recall
451 test at 24 h mice in all four experimental groups spent significantly more time exploring
452 the novel object, demonstrating integrity in a longer-term expression of the memory (Fig.
453 2C). Representative movement traces of the mice during the NOR testing are shown in
454 Figure 3.

455 **Neural stem cell-exosomes protect the hippocampus from Tau oligomer-induced**
456 **suppression of long-term potentiation expression via select miRNAs.**

457 To investigate the cellular underpinnings of NSCexo protective effects against TauO-
458 induced memory impairments, we assessed LTP expression in hippocampal slices from
459 mice injected with or without exosomes, then exposed to TauO using a well-documented
460 protocol for TauO-mediated LTP inhibition.(Dineley et al., 2010) Wild-type mice were
461 injected (ICV) with NSCexo or MNexo (1×10^9 exosomes in 3 ml of PBS) 24 h before

462 euthanasia. Hippocampal slices were prepared and incubated in HEPES solution with or
463 without pre-formed TauO (50 nM) for 1 h (Fig. 4A).

464 Following a stable 10 m baseline, slices underwent high-frequency stimulation (HFS) for
465 1 m, and LTP was recorded for 60 m. When comparing LTP expression after
466 administering NSCexo or MNexo to the control treatment with PBS, there were no
467 significant differences, with LTP expression being approximately 161% of baseline. When
468 brain slices were treated with TauO, a clear reduction in LTP expression (to 131%) was
469 observed in slices from animals previously treated with either PBS (131%) or MNexo
470 (134%). However, slices from NSCexo-treated animals showed less reduction in LTP
471 (155%) (Fig. 4B). A quantitative analysis of LTP in the final 10 m of recording (Fig. 2C)
472 confirmed a significant decline in HFS-LTP triggered by TauO in slices from animals
473 treated with PBS and MNexo, but not in slices from animals treated with NSCexo. Thus,
474 given their potential role in memory protection, NSCexo appears to diminish the
475 vulnerability of hippocampal synapses to TauO-induced LTP disruption. We also
476 observed a trend of reduction without significance in the synaptic strength attributed to
477 the toxic effects of TauO on the slope and on the FV as seen with MNexo (Fig. 5).

478 We have previously reported that specific miRNAs enriched in NSCexo as compared to
479 MNexo (miR-17, miR-322, miR-485) render synapses physically resistant to the
480 detrimental binding of AbO and functionally resilient to their disruptive action. (Micci et al.,
481 2019) To test whether these miRNAs can also protect the hippocampus against TauO-
482 suppression of LTP, wild-type mice received ICV injections of mimics for three miRNAs
483 (miR-485, miR-17, and miR-322) or an equal amount of scrambled RNA as control. Mice
484 were euthanized 24 h later and hippocampal slices were prepared and treated for 1 h with
485 preformed TauO (50 nM) or PBS (Fig. 6A). After a stable baseline of 10 min, slices were
486 subjected to high-frequency stimulation (HFS) for 1 m, and LTP was measured for 1 h
487 after that. We found that TauO-driven reduction of LTP was absent in mice treated with
488 miRNA mimics (Fig. 6B-C). Proper target engagement for the miRNAs was confirmed by
489 RT-qPCR in a separate set of experiments, as previously reported. (Micci et al., 2019)

490 **Intracerebroventricular delivery of neural stem cell exosomes prevent neuronal**
491 **accumulation of Tau oligomers in the hippocampus and cortex.**

492 At the end of NOR testing, mice were euthanized, perfused with PBS, and fixed in 4%
493 paraformaldehyde. The brains were processed for Tau and pTau immunofluorescence
494 analyses (refer to Fig. 1A for the experimental design). We found that significantly less
495 Tau and pTau were present in the hippocampus (dentate gyrus, CA1, and CA3) of mice
496 that received NSCexo ICV as compared to PBS and MNexo injected mice (Fig. 7).
497 Moreover, we observed reduced levels of Tau and pTau in the parietal and frontal cortex
498 of NSCexo-treated mice compared with those treated with MNexo and PBS (Fig. 8).

499 **Neural stem cell exosomes reduce the internalization of Tau oligomers into** 500 **synaptosomes.**

501 Because of the observed protective effects of NSCexo on TauO-induced memory
502 disruption and inhibition of LTP expression, we explored whether exosomes released by
503 hippocampal NSCs could mitigate synaptic susceptibility to TauO. Synaptosomes were
504 isolated from the hippocampus of mice previously injected (ICV) with PBS or exosomes
505 (NSCexo or MNexo) and incubated for 1 h with preformed TauO (5 nM). After washing
506 away excess Tau, synaptosomes were incubated for 30 m with PK, to remove surface-
507 bound Tau, or vehicle. Internalized and total content of Tau was determined by ELISA
508 (see schematic, Fig. 9A). We found that the amount of total Tau (internalized and at the
509 surface) in hippocampal synaptosomes was not significantly different between the
510 experimental groups (Figure 9B). However, after PK treatment, the amount of TauO
511 measured in hippocampal synaptosomes isolated from mice treated with NSCexo was
512 significantly reduced compared to synaptosomes from mice treated with PBS or MNexo
513 ($p < 0.01$ NSCexo vs PBS, $p < 0.05$ NSCexo vs MNexo) (Fig. 9C). This suggests that
514 NSCexo reduces TauO internalization but not binding at the synaptosome surface.

515 To further determine the effect of NSCexo on TauO binding and internalization in the
516 synapses, synaptosomes were incubated with increasing concentrations of labeled
517 TauO488 (25, 50, 250, 500, 1000 nM) in the presence or absence of PK and analyzed by
518 flow cytometry (see schematic in Fig. 10A). Our results revealed a dose-dependent
519 increase in both the percentage of TauO-positive synaptosomes (Fig. 10B) and the
520 amount of TauO bound to synaptosomes expressed as Median Fluorescence Intensity
521 (MFI) (Fig. 10D) across all experimental groups (PBS, NSCexo, and MNexo). However

522 following PK treatment, a greater reduction in TauO positivity was observed in
523 synaptosomes isolated from NSCexo-treated mice at the TauO 50 nM concentration
524 compared to synaptosomes from MNexo-treated mice (Fig. 10C). Additionally, we
525 observed a greater reduction in TauO MFI in NSCexo-treated mouse synaptosomes
526 compared to those from PBS-treated mice at 25 and 250 nM TauO, as well as MNexo-
527 treated mouse synaptosomes at 25 nM TauO (Fig. 10E). When we compared the
528 outcomes of PK-digested samples with their respective control conditions (without PK)
529 for each TauO concentration (Fig. 11), we found that synaptosomes from NSCexo-treated
530 mice, exposed to 25 nM TauO concentration, exhibited a significantly lower percentage
531 of TauO-positive synaptosomes after PK digestion compared to synaptosomes treated
532 with PBS or MNexo, relative to their respective control groups. (Fig. 11B). No differences
533 between the groups were noted in the percentage of synaptosomes positive for TauO
534 before and after PK treatment at higher TauO concentrations (50, 250, 500, 1000 nM)
535 (Fig. 11C-F).

536 Interestingly, when we compared the amount of TauO (MFI) before and after PK
537 treatment, we found significantly lower levels of TauO after PK in synaptosomes from
538 NSCexo-treated mice but not in those from PBS- and MNexo-treated mice at all Tau
539 concentrations tested (Fig. 11G-K). These data suggest that synaptosomes isolated from
540 PBS or MNexo-treated mice, internalize most, if not all, TauO; while synaptosomes from
541 NSCexo-treated mice do not internalize TauO, so most remains bound to the outer
542 surface. Taken together, the ELISA and flow cytometry data suggest that NSCexo
543 reduces TauO internalization at the synapse without affecting TauO binding at the
544 surface.

545 **NSCexo reduce TauO internalization in hippocampal neurons *in vitro*.**

546 To test whether NSCexo-mediated reduction of TauO internalization at the synapse
547 resulted from a direct effect on neurons, we exposed cultures of mature hippocampal
548 neurons, generated from NSC differentiation, to NSCexo or MNexo for 24 h. After
549 removing excess exosomes, TauO (2.5 mM) was added to the cultures for 60 m, and the
550 cells were washed, fixed, and stained with anti-βIII-tubulin and anti-hTau (Tau5)
551 antibodies. Confocal images revealed the presence of Tau bound to the dendritic

552 processes and within the cell bodies (as previously reported)(Puangmalai et al., 2020)
553 (Figure 12A-C). Quantitative analysis showed that, while TauO did not reduce the number
554 of neurons (Fig 13A), NSCexo treatment significantly reduced the amount of Tau found
555 inside the neurons, specifically in the nucleus (Fig. 12D), and increased the number of
556 neurites without TauO puncta (Fig. 6E). The number of Tau puncta per neurites was
557 reduced in both NSCexo- and MNexo-treated neurons as compared to those treated with
558 PBS (Fig. 12F). No puncta were visible in cultures not treated with TauO (Ctrl) and stained
559 with anti-hTau antibody (Fig. 13B). These results suggest that NSCexo reduced the
560 internalization of Tau into neurons (in accordance with the ELISA and flow cytometry data
561 and the in vivo immunofluorescence data).

562

JNeurosci Accepted Manuscript

563 Discussion

564 Neural stem cells (NSC) are critical for neurogenesis in the hippocampus, a process
565 necessary for synaptic plasticity, learning and memory.(Kempermann et al., 2018)
566 Previously, we showed that aged individuals who remained cognitively intact despite the
567 presence of A β plaques and tau tangles in the brain, had high numbers of NSCs in the
568 hippocampus.(Briley et al., 2016) Consistent with this discovery, we showed that
569 exosomes released by hippocampal NSCs reduced the binding of A β O at synapses and
570 prevented A β O-induced suppression of LTP and memory recall deficits.(Micci et al.,
571 2019)

572 Here, we report, in wild-type mice, that NSCexo reduced internalization of TauO into
573 hippocampal neurons, protected synapses from TauO-induced suppression of LTP
574 expression, and prevented memory deficits driven by ICV injection of TauO. and that
575 these effects may occur via delivery of specific miRNA exosomal cargo. Most importantly,
576 we show that this mechanism is specific to NSCexo because exosomes secreted by MN,
577 generated from the differentiation of hippocampal NSCs, were unable to provide similar
578 protections. Using exosomes from MNs derived from differentiation of NSCs, enables the
579 comparison of exosomes specifically associated with both a "stem" state and a mature
580 neuronal phenotype within the same cell lineage. Consequently, this approach excludes
581 the potential of non-specific effects of exosome vesicles, such as scavenging of
582 exogenously-added TauO.(An et al., 2013; Yuyama et al., 2015)

583 Our data show that both synaptic plasticity (LTP) and memory (NOR) can be protected
584 against TauO-induced deficits in mice treated with NSCexo prior to challenging with
585 TauO. These results indicate that exosomes released by hippocampal NSCs play a key
586 role in promoting or maintaining synaptic resistance to the damaging effects of TauO that
587 ultimately result in memory deficits. Comparable trend of fEPSP reduction was observed
588 following TauO application in PBS or NSCexo-treated animals, which was greater in the
589 MNexo group where a significant effect is observed with the fiber volley that will be
590 explored in the future. This data suggests other mechanisms than a direct effect on
591 synaptic strength via action of NSCexo is involved with improvement of cognitive
592 response observed.

593 Our data show that ICV injection of TauO impair short-term memory but not long-term
594 memory in the NOR test. This may be explained by their preferential impact on
595 hippocampal synaptic plasticity and function, which are critical for short-term memory
596 consolidation.

597 Tau oligomers are known to disrupt synaptic integrity, impair long-term potentiation (LTP),
598 and alter neuronal communication in the hippocampus. These disruptions can selectively
599 affect the encoding and retrieval of short-term memory, which relies heavily on intact
600 hippocampal circuits. Conversely, long-term memory may involve broader cortical
601 networks and compensatory mechanisms that are less immediately impacted by acute
602 toxic effects of TauO ICV injection.

603 Our data show that ICV injection of NSCexo, but not MNexo, prior to TauO delivery,
604 reduces Tau and pTau accumulation in the hippocampus and cortex. Our previously
605 published data showed that exosomes are taken up by neurons. Here we show that
606 NSCexo can reduce TauO internalization when administered to neuronal cultures. The
607 possibility that NSCexo are also taken up by glial cells when injected ICV cannot be
608 excluded. Further studies are necessary to determine whether this is the case and what
609 the functional significance would be.

610 TauO are known to accumulate in synapses resulting in disrupted synaptic transmission,
611 ultimately leading to dendritic spine retraction and cognitive impairments.(Tu et al.,
612 2014)(Lacor et al., 2004) Our data show that NSCexo reduce TauO internalization into
613 isolated synaptosomes and cultured hippocampal neurons. The mechanisms remain
614 unclear, they may involve the low-density lipoprotein receptor-related protein 1 (LRP1).
615 LRP1 is abundantly expressed at synapses and has been recently shown to function as
616 a major transporter for TauO allowing rapid internalization of Tau and its subsequent
617 spreading.(Rauch et al., 2020; Cooper et al., 2021) Our data are consistent with the idea
618 that an action of the cargo of NSCexo on the LRP1-Tau complex could be responsible
619 for reduced Tau internalization but unaffected tau surface binding in synaptosomes of
620 NSCexo-treated mice.

621 MiRNAs are abundant in exosomes and, in addition to proteins and lipids, represent their
622 main bioactive cargo.(van den Boorn et al., 2013; Bayraktar et al., 2017) Indeed,

623 compelling evidence indicates that many of the effects elicited by exosomes (including
624 NSCexo) can be ascribed to the action of their specific miRNA cargoes, including
625 modulation of aging,(Zhang et al., 2017) cognition and synaptic function(Hebert et al.,
626 2009; Konecna et al., 2009; Cohen et al., 2011) and neuroprotection.(Properzi et al.,
627 2015) Importantly, miRNAs have been shown to regulate transcriptional modulation of
628 key synaptic proteins within the synaptic compartment itself.(Schratt, 2009; Garza-
629 Manero et al., 2014) Furthermore, our own previous findings show that resilient
630 hippocampal synapses in NDAN individuals with high numbers of NSCs(Briley et al.,
631 2016) have a unique proteomic signature,(Zolochavska et al., 2018) suggesting that
632 selective changes in synaptic protein expression mark synaptic resistance to toxic A β O
633 and TauO in these humans. This is consistent with upstream regulation by specific
634 miRNAs, as revealed by IPA analysis of our proteomic data. We have previously shown
635 that, compared to MNexo, NSCexo contain a unique set of miRNAs that are known to
636 modulate the expression of proteins involved in synaptic function.(Micci et al., 2019) Most
637 importantly, we also found that when injected ICV in mice, mimics of such unique
638 NSCexo-derived miRNAs render synapses physically resistant to the detrimental binding
639 of A β O and functionally resilient to their disruptive action. Here we demonstrated that
640 these unique NSCexo-derived miRNAs protect mice from TauO-induced LTP and
641 memory dysfunctions. These data further support the notion that selected miRNAs
642 uniquely present in NSCexo mediate their protective action on synapses of target neurons
643 and further suggest the exciting possibility of new drug discovery to promote cognitive
644 resilience in patients with Alzheimer's disease.

645 Our data point to NSC-secreted exosomes, and their miRNA cargo, as critical elements
646 of the, yet poorly understood, neurobiological basis of the relationship between brain
647 reserve, cognitive resilience, and resistance to Alzheimer's disease neuropathology.
648 While the relative quantity of exosomes released by NSC in the hippocampus is not
649 known, we know that exosomes injected in the dentate gyrus can spread to other regions
650 of the hippocampus and to the cortex.(Zheng et al., 2017) An intriguing possibility is that
651 a decrease in the number of NSCs in the hippocampal dentate gyrus, such as that which
652 occurs during aging,(Kuhn et al., 2007; Ben Abdallah et al., 2010; Lugert et al., 2010)
653 could lead to increased synaptic vulnerability to the toxic binding of A β O and TauO,

654 because of reduced NSCexo in the hippocampus. Such a mechanism could be one factor
655 that links aging to increased risk of Alzheimer's disease.(Querfurth and LaFerla, 2010)

656 The future pursuit of this novel concept has the potential to open the door to new
657 therapeutic strategies for Alzheimer's disease centered on NSC-secreted exosomes and
658 their bioactive cargo. Indeed, our previous reports and the results of this work,
659 demonstrating the effect of NSC-secreted exosomes in increasing synaptic resistance to
660 AbOs and TauO, support this possibility. NSC-secreted exosomes could delay the onset
661 and/or mitigate the severity of A β O- and TauO-dependent synaptic and cognitive
662 dysfunctions associated with age-dependent decreases in neurogenesis.

JNeurosci Accepted Manuscript

663

664 **Availability of data and materials:** Raw data is available from the corresponding
665 authors upon reasonable request.

666 **Funding:** Supported by NIA/NIH 5R01AG042890 (to MAM and GT)

667

JNeurosci Accepted Manuscript

668 **References**

- 669 Altman J, Das GD (1965) Autoradiographic and histological evidence of postnatal hippocampal
670 neurogenesis in rats. *J Comp Neurol* 124:319-335.
- 671 An K, Klyubin I, Kim Y, Jung JH, Mably AJ, O'Dowd ST, Lynch T, Kanmert D, Lemere CA, Finan
672 GM, Park JW, Kim TW, Walsh DM, Rowan MJ, Kim JH (2013) Exosomes neutralize
673 synaptic-plasticity-disrupting activity of Abeta assemblies in vivo. *Mol Brain* 6:47.
- 674 Appel J, Potter E, Shen Q, Pantol G, Greig MT, Loewenstein D, Duara R (2009) A comparative
675 analysis of structural brain MRI in the diagnosis of Alzheimer's disease. *Behav Neurol*
676 21:13-19.
- 677 Barnes J, Bartlett JW, van de Pol LA, Loy CT, Scahill RI, Frost C, Thompson P, Fox NC (2009)
678 A meta-analysis of hippocampal atrophy rates in Alzheimer's disease. *Neurobiol Aging*
679 30:1711-1723.
- 680 Baulch JE, Acharya MM, Allen BD, Ru N, Chmielewski NN, Martirosian V, Giedzinski E, Syage
681 A, Park AL, Benke SN, Parihar VK, Limoli CL (2016) Cranial grafting of stem cell-derived
682 microvesicles improves cognition and reduces neuropathology in the irradiated brain.
683 *Proc Natl Acad Sci U S A* 113:4836-4841.
- 684 Bayraktar R, Van Roosbroeck K, Calin GA (2017) Cell-to-cell communication: microRNAs as
685 hormones. *Mol Oncol* 11:1673-1686.
- 686 Ben Abdallah NM, Slomianka L, Vyssotski AL, Lipp HP (2010) Early age-related changes in
687 adult hippocampal neurogenesis in C57 mice. *Neurobiol Aging* 31:151-161.
- 688 Bjorklund NL, Reese LC, Sadagoparamanujam VM, Ghirardi V, Woltjer RL, Tagliatela G
689 (2012) Absence of amyloid beta oligomers at the postsynapse and regulated synaptic
690 Zn²⁺ in cognitively intact aged individuals with Alzheimer's disease neuropathology. *Mol*
691 *Neurodegener* 7:23.
- 692 Briley D, Ghirardi V, Woltjer R, Renck A, Zolochovska O, Tagliatela G, Micci MA (2016)
693 Preserved neurogenesis in non-demented individuals with AD neuropathology. *Sci Rep*
694 6:27812.
- 695 Buenz EJ, Sauer BM, Lafrance-Corey RG, Deb C, Denic A, German CL, Howe CL (2009)
696 Apoptosis of hippocampal pyramidal neurons is virus independent in a mouse model of
697 acute neurovirulent picornavirus infection. *Am J Pathol* 175:668-684.
- 698 Bussian TJ, Aziz A, Meyer CF, Swenson BL, van Deursen JM, Baker DJ (2018) Clearance of
699 senescent glial cells prevents tau-dependent pathology and cognitive decline. *Nature*
700 562:578-582.
- 701 Clark WG, Vivonia CA, Baxter CF (1968) Accurate freehand injection into the lateral brain
702 ventricle of the conscious mouse. *J Appl Physiol* 25:319-321.
- 703 Cohen JE, Lee PR, Chen S, Li W, Fields RD (2011) MicroRNA regulation of homeostatic
704 synaptic plasticity. *Proc Natl Acad Sci U S A* 108:11650-11655.
- 705 Comerota MM, Krishnan B, Tagliatela G (2017) Near infrared light decreases synaptic
706 vulnerability to amyloid beta oligomers. *Sci Rep* 7:15012.

707 Cooper JM, Lathuiliere A, Migliorini M, Arai AL, Wani MM, Dujardin S, Muratoglu SC, Hyman
708 BT, Strickland DK (2021) Regulation of tau internalization, degradation, and seeding by
709 LRP1 reveals multiple pathways for tau catabolism. *J Biol Chem* 296:100715.

710 Cui GH, Wu J, Mou FF, Xie WH, Wang FB, Wang QL, Fang J, Xu YW, Dong YR, Liu JR, Guo
711 HD (2018) Exosomes derived from hypoxia-preconditioned mesenchymal stromal cells
712 ameliorate cognitive decline by rescuing synaptic dysfunction and regulating
713 inflammatory responses in APP/PS1 mice. *FASEB J* 32:654-668.

714 deToledo-Morrell L, Stoub TR, Wang C (2007) Hippocampal atrophy and disconnection in
715 incipient and mild Alzheimer's disease. *Prog Brain Res* 163:741-753.

716 Dineley KT, Kaye R, Neugebauer V, Fu Y, Zhang W, Reese LC, Tagliatela G (2010)
717 Amyloid-beta oligomers impair fear conditioned memory in a calcineurin-dependent
718 fashion in mice. *J Neurosci Res* 88:2923-2932.

719 Fa M et al. (2016) Extracellular Tau Oligomers Produce An Immediate Impairment of LTP and
720 Memory. *Sci Rep* 6:19393.

721 Fracassi A, Marcatti M, Tumurbaatar B, Woltjer R, Moreno S, Tagliatela G (2023) TREM2-
722 induced activation of microglia contributes to synaptic integrity in cognitively intact aged
723 individuals with Alzheimer's neuropathology. *Brain Pathol* 33:e13108.

724 Franklin W, Tagliatela G (2016) A method to determine insulin responsiveness in
725 synaptosomes isolated from frozen brain tissue. *J Neurosci Methods* 261:128-134.

726 Franklin W, Krishnan B, Tagliatela G (2019) Chronic synaptic insulin resistance after traumatic
727 brain injury abolishes insulin protection from amyloid beta and tau oligomer-induced
728 synaptic dysfunction. *Sci Rep* 9:8228.

729 Garza-Manero S, Pichardo-Casas I, Arias C, Vaca L, Zepeda A (2014) Selective distribution
730 and dynamic modulation of miRNAs in the synapse and its possible role in Alzheimer's
731 Disease. *Brain Res* 1584:80-93.

732 Gerson JE, Sengupta U, Kaye R (2017) Tau Oligomers as Pathogenic Seeds: Preparation and
733 Propagation In Vitro and In Vivo. *Methods Mol Biol* 1523:141-157.

734 Greening DW, Xu R, Ji H, Tauro BJ, Simpson RJ (2015) A protocol for exosome isolation and
735 characterization: evaluation of ultracentrifugation, density-gradient separation, and
736 immunoaffinity capture methods. *Methods Mol Biol* 1295:179-209.

737 Hamilton LK, Joppe SE, L MC, Fernandes KJ (2013) Aging and neurogenesis in the adult
738 forebrain: what we have learned and where we should go from here. *Eur J Neurosci*
739 37:1978-1986.

740 Han C, Sun X, Liu L, Jiang H, Shen Y, Xu X, Li J, Zhang G, Huang J, Lin Z, Xiong N, Wang T
741 (2016) Exosomes and Their Therapeutic Potentials of Stem Cells. *Stem Cells Int*
742 2016:7653489.

743 Hebert SS, Horre K, Nicolai L, Bergmans B, Papadopoulou AS, Delacourte A, De Strooper B
744 (2009) MicroRNA regulation of Alzheimer's Amyloid precursor protein expression.
745 *Neurobiol Dis* 33:422-428.

746 Horgusluoglu E, Nudelman K, Nho K, Saykin AJ (2017) Adult neurogenesis and
747 neurodegenerative diseases: A systems biology perspective. *Am J Med Genet B*
748 *Neuropsychiatr Genet* 174:93-112.

749 Kempermann G, Gage FH, Aigner L, Song H, Curtis MA, Thuret S, Kuhn HG, Jessberger S,
750 Frankland PW, Cameron HA, Gould E, Hen R, Abrous DN, Toni N, Schinder AF, Zhao
751 X, Lucassen PJ, Frisen J (2018) Human Adult Neurogenesis: Evidence and Remaining
752 Questions. *Cell Stem Cell* 23:25-30.

753 Klein WL (2013) Synaptotoxic amyloid-beta oligomers: a molecular basis for the cause,
754 diagnosis, and treatment of Alzheimer's disease? *J Alzheimers Dis* 33 Suppl 1:S49-65.

755 Konecna A, Heraud JE, Schoderboeck L, Raposo AA, Kiebler MA (2009) What are the roles of
756 microRNAs at the mammalian synapse? *Neurosci Lett* 466:63-68.

757 Krishnan B, Kaye R, Tagliavola G (2018) Elevated phospholipase D isoform 1 in Alzheimer's
758 disease patients' hippocampus: Relevance to synaptic dysfunction and memory deficits.
759 *Alzheimers Dement (N Y)* 4:89-102.

760 Kuhn HG, Cooper-Kuhn CM, Boekhoorn K, Lucassen PJ (2007) Changes in neurogenesis in
761 dementia and Alzheimer mouse models: are they functionally relevant? *Eur Arch*
762 *Psychiatry Clin Neurosci* 257:281-289.

763 Lacor PN, Buniel MC, Chang L, Fernandez SJ, Gong Y, Viola KL, Lambert MP, Velasco PT,
764 Bigio EH, Finch CE, Krafft GA, Klein WL (2004) Synaptic targeting by Alzheimer's-
765 related amyloid beta oligomers. *J Neurosci* 24:10191-10200.

766 Lobb RJ, Becker M, Wen SW, Wong CS, Wiegman AP, Leimgruber A, Moller A (2015)
767 Optimized exosome isolation protocol for cell culture supernatant and human plasma. *J*
768 *Extracell Vesicles* 4:27031.

769 Lotvall J, Hill AF, Hochberg F, Buzas EI, Di Vizio D, Gardiner C, Gho YS, Kurochkin IV,
770 Mathivanan S, Quesenberry P, Sahoo S, Tahara H, Wauben MH, Witwer KW, Thery C
771 (2014) Minimal experimental requirements for definition of extracellular vesicles and their
772 functions: a position statement from the International Society for Extracellular Vesicles. *J*
773 *Extracell Vesicles* 3:26913.

774 Lugert S, Basak O, Knuckles P, Haussler U, Fabel K, Gotz M, Haas CA, Kempermann G, Taylor
775 V, Giachino C (2010) Quiescent and active hippocampal neural stem cells with distinct
776 morphologies respond selectively to physiological and pathological stimuli and aging.
777 *Cell Stem Cell* 6:445-456.

778 Marcatti M, Fracassi A, Montalbano M, Natarajan C, Krishnan B, Kaye R, Tagliavola G (2022)
779 Abeta/tau oligomer interplay at human synapses supports shifting therapeutic targets for
780 Alzheimer's disease. *Cell Mol Life Sci* 79:222.

781 Marzesco AM, Janich P, Wilsch-Brauninger M, Dubreuil V, Langenfeld K, Corbeil D, Huttner WB
782 (2005) Release of extracellular membrane particles carrying the stem cell marker
783 prominin-1 (CD133) from neural progenitors and other epithelial cells. *J Cell Sci*
784 118:2849-2858.

785 Micci MA, Krishnan B, Bishop E, Zhang WR, Guptarak J, Grant A, Zolocheska O, Tumurbaatar
786 B, Franklin W, Marino C, Widen SG, Luthra A, Kernie SG, Taglialatela G (2019)
787 Hippocampal stem cells promotes synaptic resistance to the dysfunctional impact of
788 amyloid beta oligomers via secreted exosomes. *Mol Neurodegener* 14:25.

789 Mu Y, Gage FH (2011) Adult hippocampal neurogenesis and its role in Alzheimer's disease. *Mol*
790 *Neurodegener* 6:85.

791 Ohm TG (2007) The dentate gyrus in Alzheimer's disease. *Prog Brain Res* 163:723-740.

792 Properzi F, Ferroni E, Poggi A, Vinci R (2015) The regulation of exosome function in the CNS:
793 implications for neurodegeneration. *Swiss Med Wkly* 145:w14204.

794 Puangmalai N, Bhatt N, Montalbano M, Sengupta U, Gaikwad S, Ventura F, McAllen S,
795 Ellsworth A, Garcia S, Kaye R (2020) Internalization mechanisms of brain-derived tau
796 oligomers from patients with Alzheimer's disease, progressive supranuclear palsy and
797 dementia with Lewy bodies. *Cell Death Dis* 11:314.

798 Querfurth HW, LaFerla FM (2010) Alzheimer's disease. *N Engl J Med* 362:329-344.

799 Raposo G, Stoorvogel W (2013) Extracellular vesicles: exosomes, microvesicles, and friends. *J*
800 *Cell Biol* 200:373-383.

801 Rauch JN, Luna G, Guzman E, Audouard M, Challis C, Sibih YE, Leshuk C, Hernandez I,
802 Wegmann S, Hyman BT, Gradinaru V, Kampmann M, Kosik KS (2020) LRP1 is a master
803 regulator of tau uptake and spread. *Nature* 580:381-385.

804 Sato-Kuwabara Y, Melo SA, Soares FA, Calin GA (2015) The fusion of two worlds: non-coding
805 RNAs and extracellular vesicles--diagnostic and therapeutic implications (Review). *Int J*
806 *Oncol* 46:17-27.

807 Schrott G (2009) microRNAs at the synapse. *Nat Rev Neurosci* 10:842-849.

808 Selkoe DJ, Hardy J (2016) The amyloid hypothesis of Alzheimer's disease at 25 years. *EMBO*
809 *Mol Med* 8:595-608.

810 Sengupta U, Montalbano M, McAllen S, Minuesa G, Kharas M, Kaye R (2018) Formation of
811 Toxic Oligomeric Assemblies of RNA-binding Protein: Musashi in Alzheimer's disease.
812 *Acta Neuropathol Commun* 6:113.

813 Spires-Jones TL, Hyman BT (2014) The intersection of amyloid beta and tau at synapses in
814 Alzheimer's disease. *Neuron* 82:756-771.

815 Stevanato L, Thanabalasundaram L, Vysokov N, Sinden JD (2016) Investigation of Content,
816 Stoichiometry and Transfer of miRNA from Human Neural Stem Cell Line Derived
817 Exosomes. *PLoS One* 11:e0146353.

818 Taglialatela G, Hogan D, Zhang WR, Dineley KT (2009) Intermediate- and long-term recognition
819 memory deficits in Tg2576 mice are reversed with acute calcineurin inhibition. *Behav*
820 *Brain Res* 200:95-99.

821 Ting JT, Daigle TL, Chen Q, Feng G (2014) Acute brain slice methods for adult and aging
822 animals: application of targeted patch clamp analysis and optogenetics. *Methods Mol*
823 *Biol* 1183:221-242.

824 Tu S, Okamoto S, Lipton SA, Xu H (2014) Oligomeric Abeta-induced synaptic dysfunction in
825 Alzheimer's disease. *Mol Neurodegener* 9:48.

826 van den Boorn JG, Dassler J, Coch C, Schlee M, Hartmann G (2013) Exosomes as nucleic acid
827 nanocarriers. *Adv Drug Deliv Rev* 65:331-335.

828 Wang JKT, Langfelder P, Horvath S, Palazzolo MJ (2017) Exosomes and Homeostatic Synaptic
829 Plasticity Are Linked to Each other and to Huntington's, Parkinson's, and Other
830 Neurodegenerative Diseases by Database-Enabled Analyses of Comprehensively
831 Curated Datasets. *Front Neurosci* 11:149.

832 Witwer KW, Goberdhan DC, O'Driscoll L, They C, Welsh JA, Blenkiron C, Buzas EI, Di Vizio D,
833 Erdbrugger U, Falcon-Perez JM, Fu QL, Hill AF, Lenassi M, Lotvall J, Nieuwland R,
834 Ochiya T, Rome S, Sahoo S, Zheng L (2021) Updating MISEV: Evolving the minimal
835 requirements for studies of extracellular vesicles. *J Extracell Vesicles* 10:e12182.

836 Yuyama K, Sun H, Usuki S, Sakai S, Hanamatsu H, Mioka T, Kimura N, Okada M, Tahara H,
837 Furukawa J, Fujitani N, Shinohara Y, Igarashi Y (2015) A potential function for neuronal
838 exosomes: sequestering intracerebral amyloid-beta peptide. *FEBS Lett* 589:84-88.

839 Zhang Y, Kim MS, Jia B, Yan J, Zuniga-Hertz JP, Han C, Cai D (2017) Hypothalamic stem cells
840 control ageing speed partly through exosomal miRNAs. *Nature* 548:52-57.

841 Zheng T, Pu J, Chen Y, Mao Y, Guo Z, Pan H, Zhang L, Zhang H, Sun B, Zhang B (2017)
842 Plasma Exosomes Spread and Cluster Around β -Amyloid Plaques in an Animal Model of
843 Alzheimer's Disease. *Frontiers in Aging Neuroscience* 9.

844 Zolocheska O, Tagliatela G (2016) Non-Demented Individuals with Alzheimer's Disease
845 Neuropathology: Resistance to Cognitive Decline May Reveal New Treatment
846 Strategies. *Curr Pharm Des* 22:4063-4068.

847 Zolocheska O, Bjorklund N, Woltjer R, Wiktorowicz JE, Tagliatela G (2018) Postsynaptic
848 Proteome of Non-Demented Individuals with Alzheimer's Disease Neuropathology. *J*
849 *Alzheimers Dis* 65:659-682.

850

851

852 **Figure legends**

853 **Figure 1. Figure 1 Characterization of isolated exosomes.** Schematic representation
854 of the methods used to characterize the exosome preparations. **(Left)** Representative
855 high-resolution transmission electron microscopy image of NSCexo and MNexo, isolated
856 using the ultra-centrifugation method (scale bar = 0.1 μm). **(Middle)** Representative NTA
857 profile for NSCexo and MNexo showing the size and concentration of particles. **(Right)**
858 Representative dot blot comparing exosome markers expression in NSCexo, MNexo and
859 total homogenate from mouse parietal cortex (mPC-H). NSCexo = Neural stem cells
860 exosomes; MNexo = Mature neurons exosomes; NTA = Nano tracking analysis

861 **Figure 2. TauO-induced memory deficit is rescued by NSCexo.** **(A)** Schematic of the
862 experimental design. Mice were injected (ICV) with either 1×10^9 exosomes (NSCexo or
863 MNexo) or ACSF 24 h before injection (ICV) of 3 mL of 0.55mM TauO or PBS. Four hours
864 later, they were subjected to the novel object recognition (NOR) memory test. **(B)**
865 Discrimination index during the training phase when the mice are exposed to two identical
866 objects. One-way ANOVA ($F=1.580$) and Tukey's multiple comparisons test. $n=7-10$
867 mice/group. Data is mean \pm SD. **(C)** Box plot representation of the Discrimination Index
868 calculated as the ratio between time spent with the novel object and the time spent with
869 the familiar object during the 2h and 24h memory recall tests. Two-way ANOVA of
870 repeated measure data with Dunnett multiple comparisons test versus Training. $*P<0.05$,
871 $**P<0.01$, $***P<0.005$. $n=7-10$ mice/group. Data is min-max.

872 NSCexo = neural stem cell exosomes; MNexo = mature neuronal exosomes; PBS =
873 phosphate-buffered saline; TauO = Tau oligomers; ACSF = artificial cerebrospinal fluid;
874 SD = Standard deviation

875 **Figure 3 Representative movement traces of mice during the NOR testing.**
876 Representative movement traces of mice ICV injected with either PBS, NSCexo, or
877 MNexo prior treatment with TauO or ACSF. Left panels show data from the training phase
878 of the test; middle panels show data from the 2h memory recall test; right panels show
879 data from the 24h memory recall test. N = novel object; PBS = phosphate-buffered saline;
880 NSCexo = Neural stem cells exosomes; MNexo = Mature neurons exosomes; TauO =
881 Tau oligomers; ACSF = artificial cerebrospinal fluid

882

883 **Figure 4. TauO-induced suppression of LTP expression in the hippocampus is**
884 **abolished by ICV injection of NSCexo. (A)** Schematic of the experimental design: Mice
885 were administered ICV injections of either NSCexo, MNexo, or PBS. After 24 hours, they
886 were euthanized. Brain sections from these mice were subsequently treated with or
887 without TauO. Field recordings of LTP were then conducted in the Schaffer collateral
888 region of the hippocampus. **(B and D)** Field potential recording of LTP, compared to the
889 percent of baseline, from brain slices pretreated with NSCexo but not with MNexo, in the
890 presence or absence of TauO, revealed differences in the slope of excitatory postsynaptic
891 potentials. **(C)** For each experimental condition, the amplitude of fEPSP during the final
892 10 m (from the 50th -60th min post high frequency stimulation) were averaged. TauO
893 significantly reduced LTP in brain slice taken from mice injected with either PBS or
894 MNexo. Conversely, this suppressive effect was not seen in slices from mice that received
895 the NSCexo injection. PBS: $n = 7$, NSC-exo: $n = 7$, and MN-exo: $n = 6$ (1-4 slices per
896 mouse). * $P < 0.05$ Two-way ANOVA followed by Tukey's multiple comparisons test.

897 NSCexo = neural stem cells exosomes; MNexo = mature neurons exosomes; PBS =
898 phosphate-buffered saline; TauO = Tau oligomers; LTP = long term potentiation; fEPSP
899 = functional excitatory post-synaptic potential

900 **Figure 5 Application of TauO reduces the slope while application of MNexo affects**
901 **the fiber volley.** The input-output (IO) plotted as slope (mV/ms) on the Y-axis as a
902 function of fiber volley (FV in mV) on the X-axis is provided prior to high-frequency
903 stimulation (pre-, clear circles) and after (post-, filled circles) for (A) PBS treated, (B)
904 NSCexo treated, (C) MNexo treated. The panel on the left is untreated, while the panel
905 on the right is from TauO treated. Slope for (D) PBS treated, (E) NSCexo treated, (F)
906 MNexo treated and FV as a function of stimulation (mA) for (G) PBS treated, (H) NSCexo
907 treated, (I) MNexo treated provide additional insight into the role of TauO and MNexo
908 treatment on synaptic strength.

909 **Figure 6 TauO-induced LTP suppression in the hippocampus is abolished by**
910 **mimics of miRNAs enriched in NSCexo. (A)** Schematic of the experimental design.
911 MicroRNAs (scrambled or mimics of miR-322, miR17 and miR-485) or ACSF (vehicle)

912 were injected ICV into adult mice 24 hours before euthanasia. **(B)** Schaffer collateral field
913 recording of LTP (indicated as percent of baseline in the slope of fEPSPs) was performed
914 on brain slices in the presence of TauO (50 nM) or ACSF. TauO abolished LTP in ACSF-
915 injected mice and in scrambled-treated mice but not in miRNAs combo-treated mice. **(C)**
916 Average for each condition of the fEPSP amplitude for the final 10 minutes (time points
917 50–60 minutes post high frequency stimulation). TauO significantly reduced LTP in brain
918 slices from mice injected with vehicle or with scrambled miRNA, but not in brain slices
919 from mice treated with combo miRNAs mimics. N=4 mice/group (3 slices per mouse).
920 ** $P < 0.01$; **** $P < 0.0001$ one-way ANOVA followed by Dunnett's multiple comparisons test.
921 ACSF = artificial cerebrospinal fluid; ICV = intracerebroventricular; LTP = long-term
922 potentiation; fEPSPs = functional excitatory post-synaptic potentials; TauO = Tau
923 oligomers

924
925 **Figure 7. NSCexo reduce Tau and pTau accumulation in the hippocampus.**
926 Representative images and quantitative analyses of triple immunofluorescence staining
927 for NeuN (magenta) in combination with total Tau (red) and pTau (AT8-green) revealed
928 a significant decrease in Tau and pTau levels after treatment with NSCexo in DG, CA1
929 and CA3. Scale bar 20 μ m. Statistical analyses were made using one-way analysis of
930 variance, following Tukey's multiple comparisons test. Values are expressed as the mean
931 \pm SD. * $P \leq 0.05$, ** $P \leq 0.01$, *** $P \leq 0.001$.

932 NeuN = neuronal nuclei; NSCexo = neural stem cells exosomes; DG = dentate gyrus

933 **Figure 8 NSCexo reduce Tau and pTau accumulation in the cortex.** Representative
934 images and quantitative analyses of triple immunofluorescence staining for NeuN
935 (magenta) in combination with total Tau (red) and pTau (AT8-green) revealed a significant
936 decrease in Tau and pTau levels after treatment with NSCexo in both parietal and frontal
937 cortex. Scale bar 20 μ m. Statistical analyses were made using one-way analysis of
938 variance, following Tukey's multiple comparisons test. Values are expressed as the mean
939 \pm SD. * $P \leq 0.05$, ** $P \leq 0.01$, *** $P \leq 0.001$. NeuN = neuronal nuclei; NSCexo = neural stem
940 cells exosomes; SD = standard deviation

941

942 **Figure 9. NSCexo reduce hippocampal synaptic vulnerability to TauO.** Exosomes
943 (NSCexo or MNexo) or PBS were injected ICV 24hr before sacrifice. Brain synaptosomes
944 were prepared from the hippocampus and challenged with preformed 5 nM TauO for 1h
945 followed by treatment with PK or vehicle for 30 minutes. After washing, the amount of
946 TauO bound to synaptosomes was quantified by ELISA. **(A)** Schematic of the
947 experimental design; **(B)** quantification of total tau; **(C)** quantification of internalized tau
948 after PK treatment. $n=8$ mice/group (average of two independent experiments). $*P<0.05$;
949 $**P<0.01$ vs. PBS Unpaired T-test. Data is median.

950 NSCexo = neural stem cells exosomes; MNexo = mature neurons exosomes; PBS =
951 phosphate-buffered saline; TauO = Tau oligomers; PK = proteinase K

952 **Figure 10. Effect of NSCexo on synaptic TauO binding and internalization.**
953 Exosomes (NSCexo or MNexo) or PBS were injected ICV 24 hours before sacrifice.
954 Synaptosomes were isolated from the hippocampus and challenged with preformed
955 labeled TauO488 at increasing concentrations or PBS for 1 hour. After washing,
956 synaptosomes were treated with PK or vehicle for 30 minutes, washed and analyzed by
957 flow cytometry. **(A)** Schematic of the experimental design; **(B-C)** Percentage of
958 synaptosomes positive for TauO488 with and without PK treatment. **(D-E)** Median
959 Fluorescence Intensity (MFI) of TauO488-positive synaptosomes with and without PK.
960 Comparisons were performed within each group between data in the presence or
961 absence of PK. $*p<0.05$ (Multiple unpaired T-test). Synaptosomes were pooled from 8
962 individual mice per group. $N=3$ flow cytometry runs. Data is mean \pm SD.

963 NSCexo = neural stem cells exosomes; MNexo = mature neurons exosomes; PBS =
964 phosphate-buffered saline; TauO = Tau oligomers; PK = proteinase K; SD = standard
965 deviation

966

967 **Figure 11. NSCexo reduce the internalization of TauO into synaptosomes. (A)**
968 Schematic of the experimental design. **(B-F)** Flow cytometric analysis of the percentage
969 of TauO488-positive synaptosomes (after challenged with increasing concentration of
970 TauO) derived from NSCexo-, MNexo-, or PBS-treated mice before and after PK
971 digestion. **(G-K)** Flow cytometric analysis of the MFI of TauO488-positive synaptosomes

972 derived from NSCexo-, MNexo-, or PBS-treated mice before and after PK digestion.
973 * $P < 0.05$ 2-way ANOVA followed by Tukey's multiple comparison tests. Synaptosomes
974 were pooled from 8 individual mice per group. $n = 3$ flow cytometry runs. Data is mean +/-
975 SD.

976 NSCexo = neural stem cells exosomes; MNexo = mature neurons exosomes; PBS =
977 phosphate-buffered saline; TauO = Tau oligomers; PK = proteinase K

978 **Figure 12. NSCexo reduce TauO internalization into hippocampus neurons *in vitro*.**

979 Hippocampal neurons generated by differentiation of adult rat hippocampus NSC were
980 treated with NSCexo, MNexo or PBS for 24 hours before being challenged with TauO
981 (2.5 mM) for 1 hour. **(A)** Representative confocal images (60X w/ 2 zoom) of neurons
982 pre-treated with PBS, NSCexo, and MNexo (hTau in red, β III-tubulin in green, and the
983 nuclei in blue; scale bar 20 μ m). **(B)** Representative confocal images (60X w/7.5 zoom)
984 showing the presence of hTau inside the neurites (scale bar is 2 μ m). **(C)** Representative
985 confocal images (60X w/7.5 zoom) showing the presence of hTau in the neuronal cell
986 bodies (scale bar 5 μ m). **(D)** Quantification of the number of hTau puncta inside neurons
987 (5 images acquired from 8 independent experiments). * $p < 0.05$; ** $p < 0.01$ one-way
988 ANOVA ($F = 6.701$) followed by Tukey's multiple comparisons test. **(E)** Quantification of
989 the number of neurites without hTau puncta (5 images acquired from 5 independent
990 experiments). * $p < 0.05$; **** $p < 0.0001$ one-way ANOVA ($F = 22.82$) followed by Tukey's
991 multiple comparisons test. **(F)** Quantification of the number of hTau puncta on neurites (5
992 images acquired from 5 independent experiments). * $P < 0.05$; ** $P < 0.01$ one-way ANOVA
993 ($F = 7.975$) followed by Tukey's multiple comparisons test. Data is mean +/- SEM.

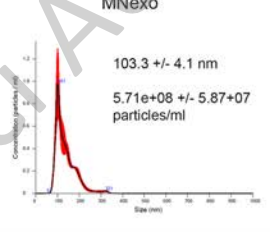
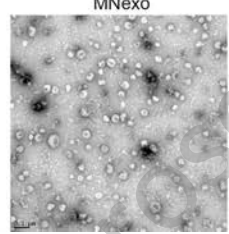
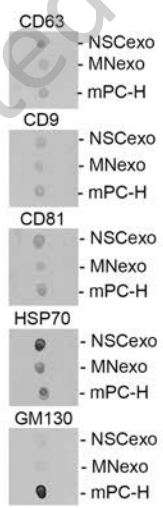
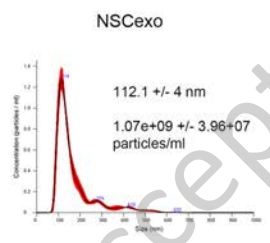
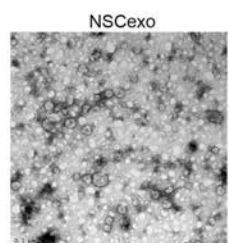
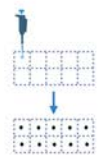
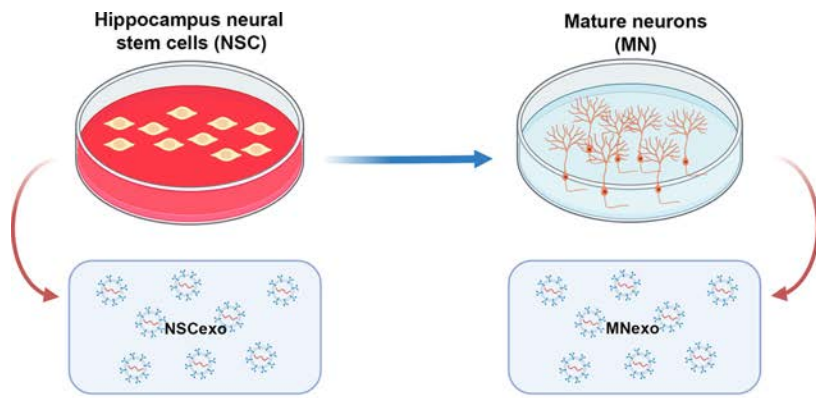
994 NSCexo = neural stem cells exosomes; MNexo = mature neurons exosomes; PBS =
995 phosphate-buffered saline; TauO = Tau oligomers; SEM = standard error of the mean

996 **Figure 13 (A)** Hippocampal neurons generated by differentiation of adult rat hippocampus
997 NSC were treated with PBS for 24 hours before being incubated with PBS for 1 hour.
998 Neurons were fixed and processed for immunofluorescence analysis using anti-hTau
999 antibody and anti- β III-tubulin. **(Left)** Representative confocal images (460X w/ 2 zoom)
1000 of neurons pre-treated with PBS (hTau in red, β III-tubulin in green, and the nuclei in blue;
1001 scale bar 20 μ m). **(Middle)** Representative confocal images (60X w/7.5 zoom) showing

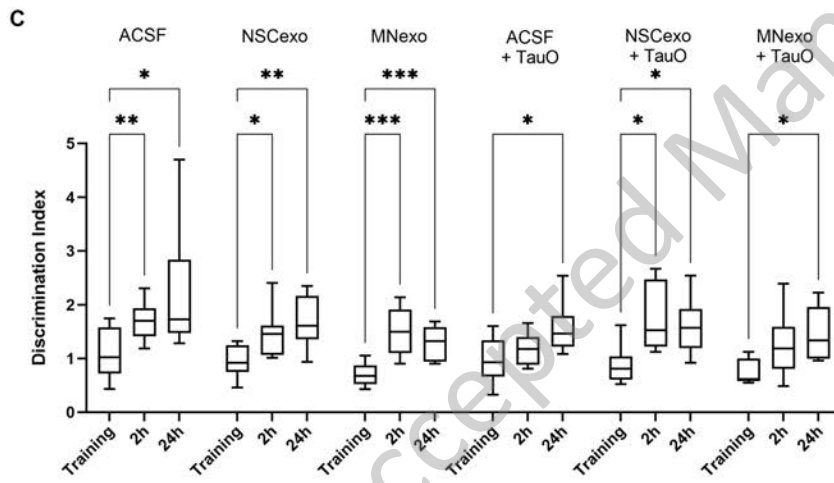
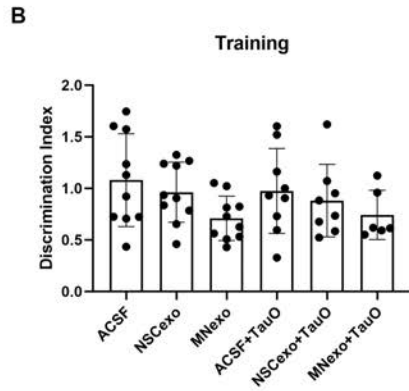
1002 the absence of hTau inside the neurites (scale bar 2 μ m). **(Right)** Representative confocal
1003 images (60X w/7.5 zoom) showing the absence of hTau in the neuronal cell bodies (scale
1004 bar is 5 μ m). NSC = neural stem cells; PBS = phosphate-buffered saline

1005 **(B)** Quantification of the number of DAPI+ cells across the experimental groups (5 images
1006 acquired from 8 independent experiments). One-way ANOVA ($F = 1.035$) followed by
1007 Tukey's multiple comparisons test.

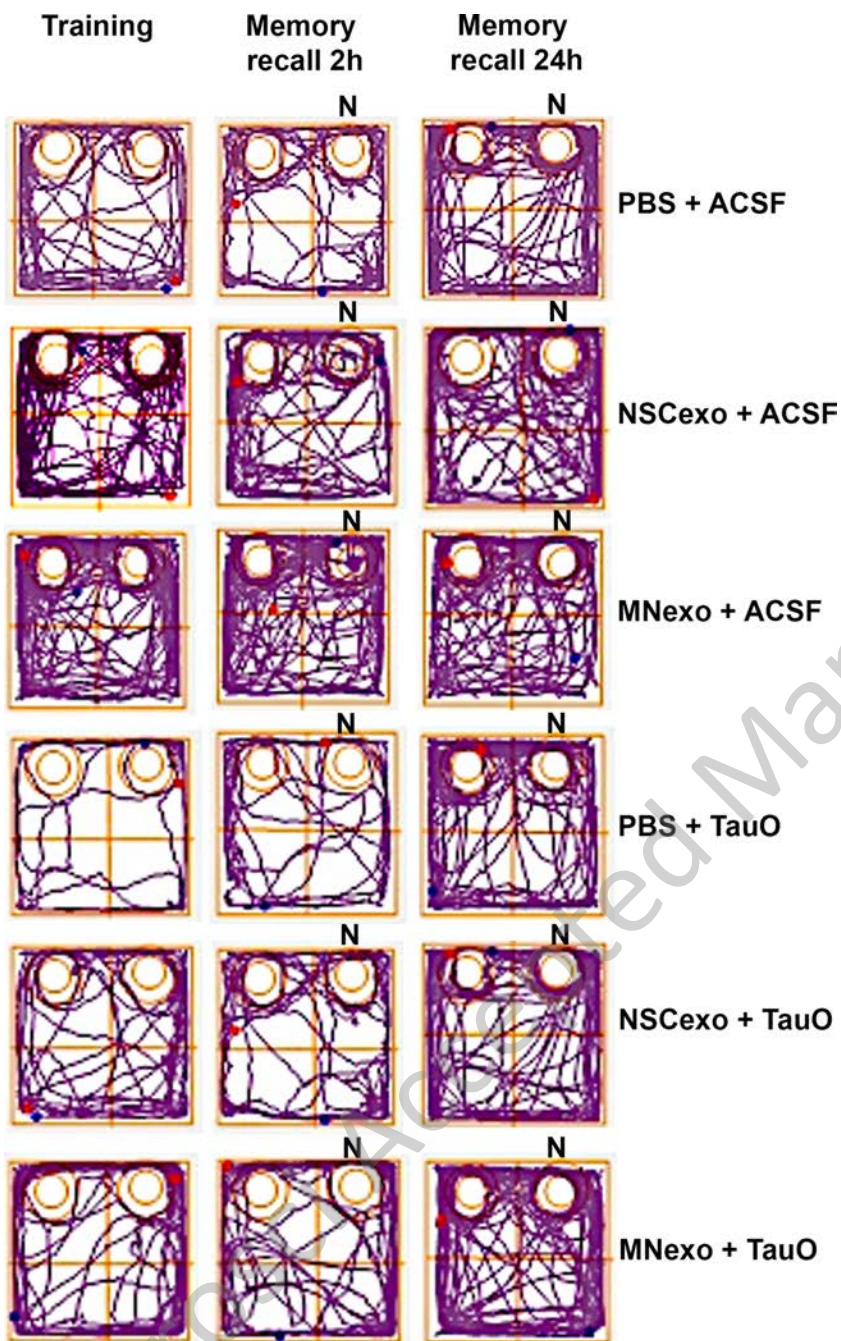
JNeurosci Accepted Manuscript



JNeurosci Accepted Manuscript



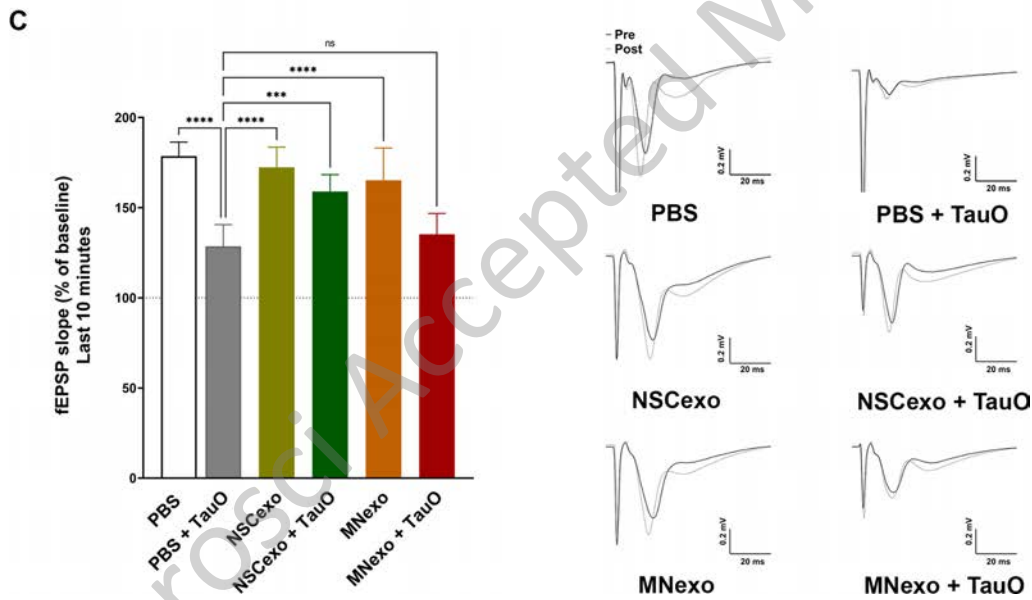
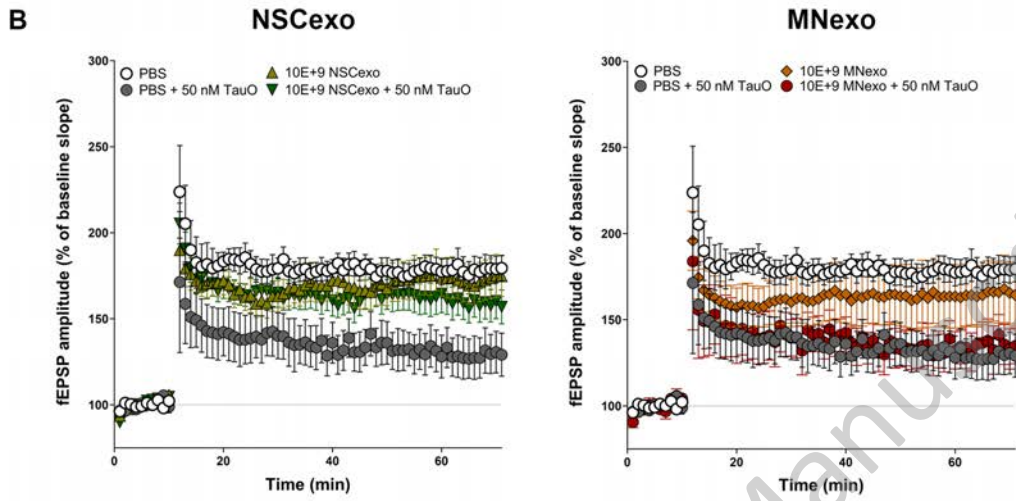
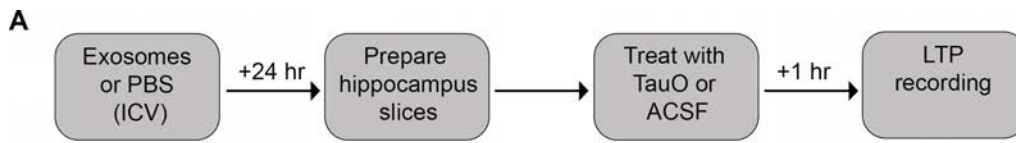
JNeurosci Accepted Manuscript

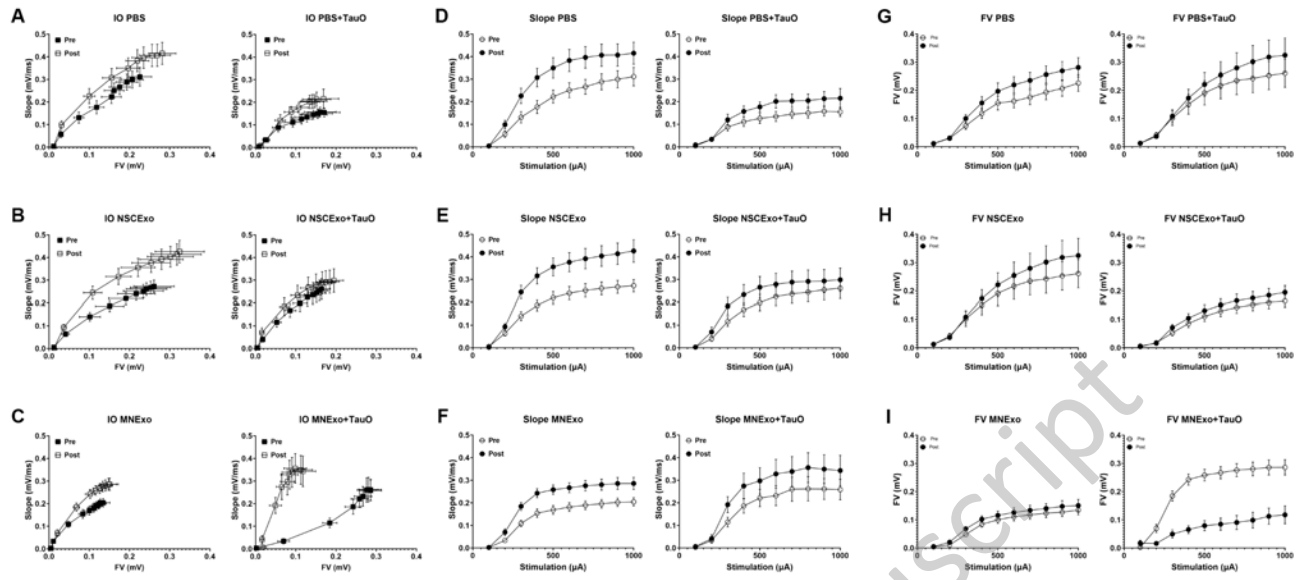


JNeurosci. 2019.11.14.367000. doi:10.1523/JNEUROSCI.3670-19.2019

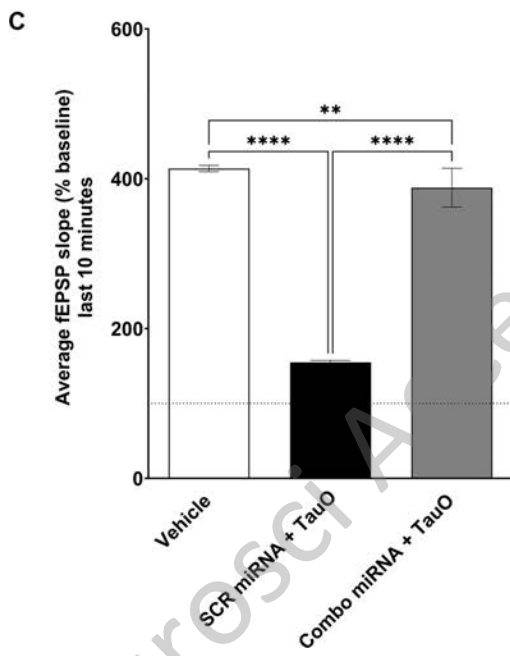
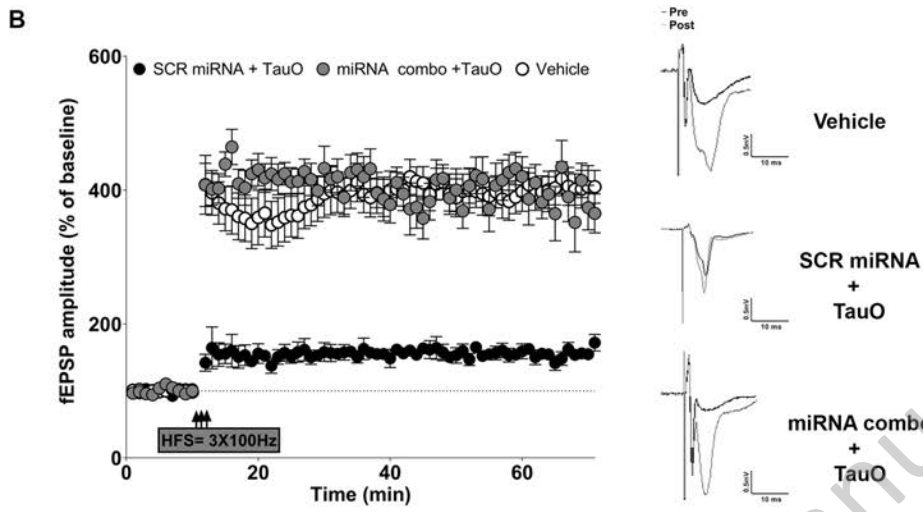
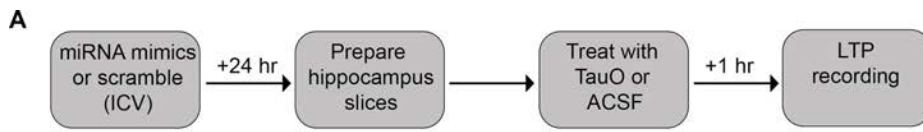
Preprint

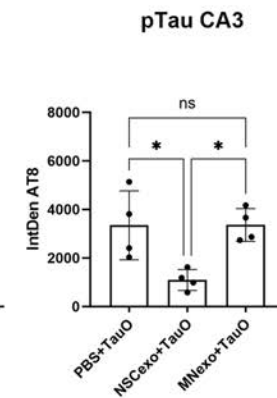
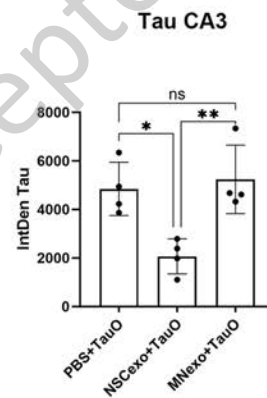
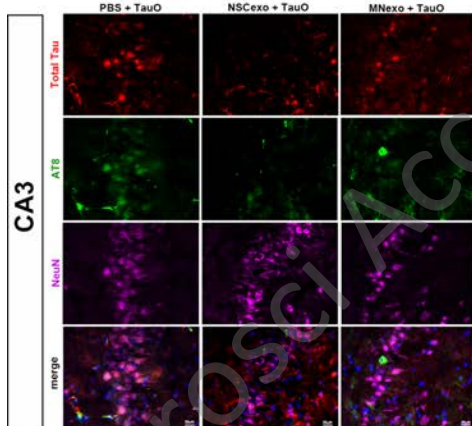
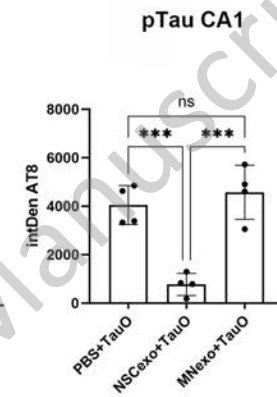
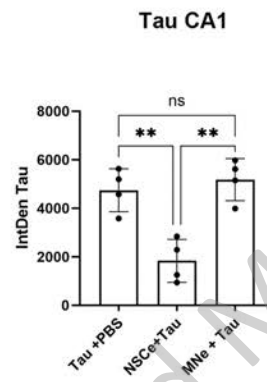
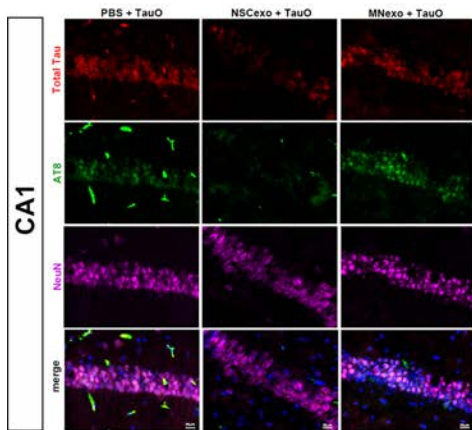
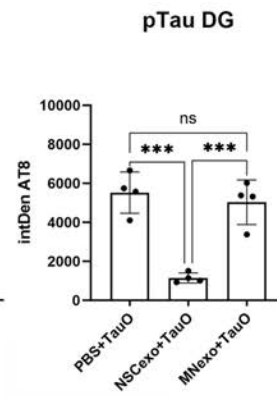
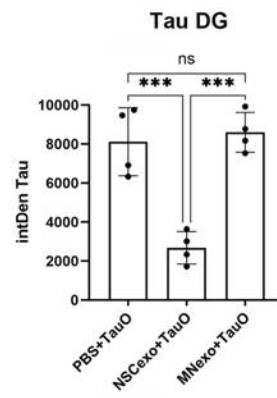
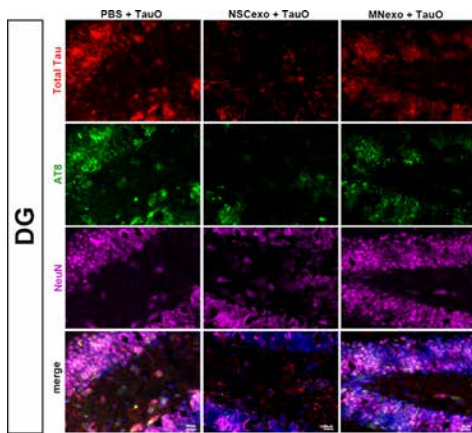
Manuscript



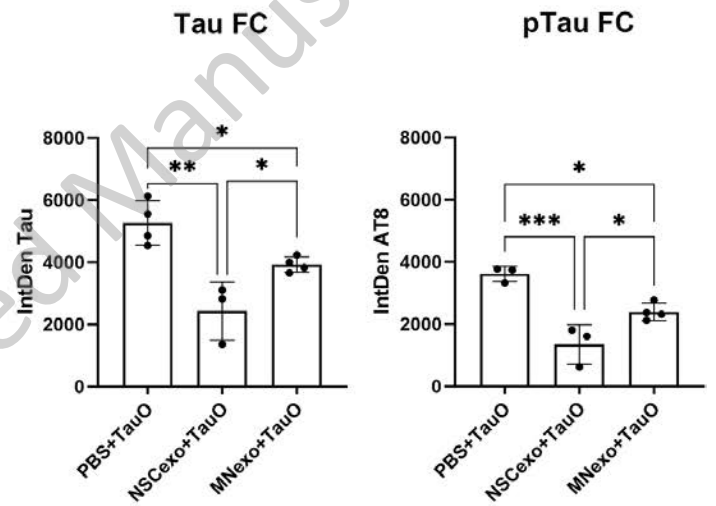
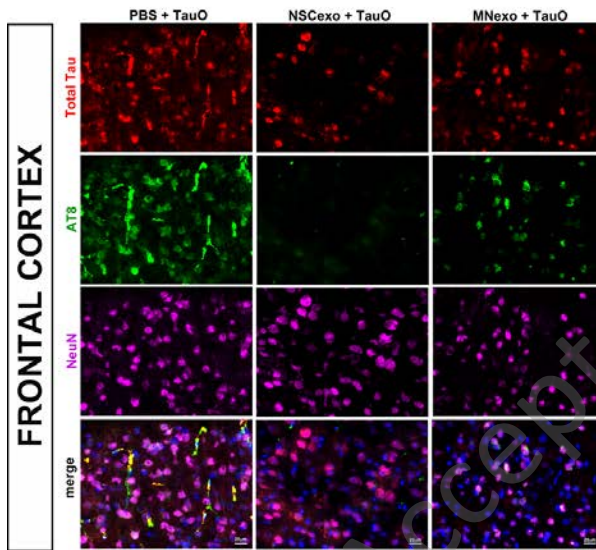
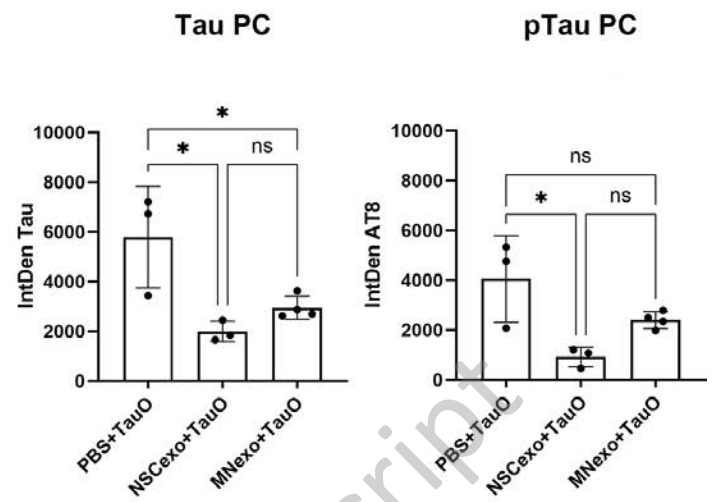
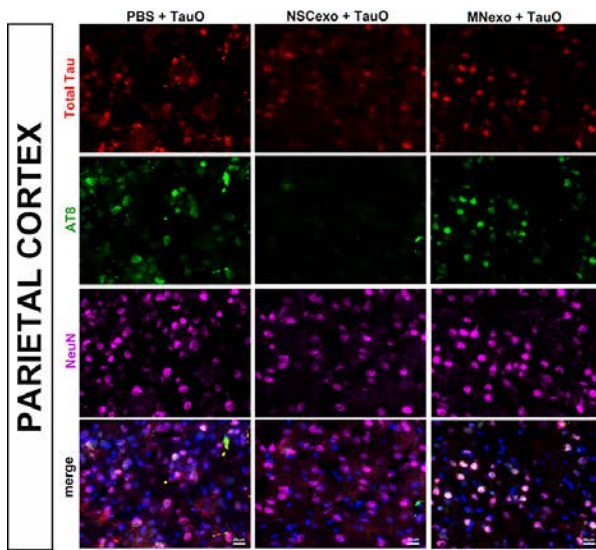


JNeurosci Accepted Manuscript

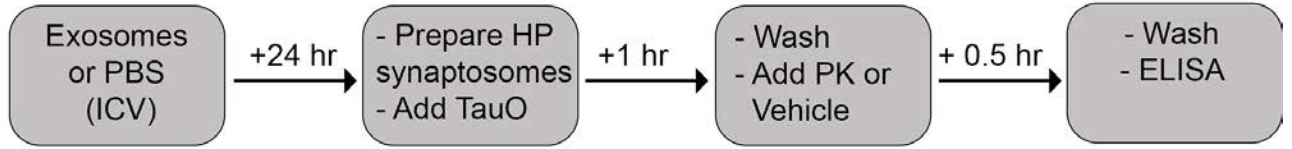
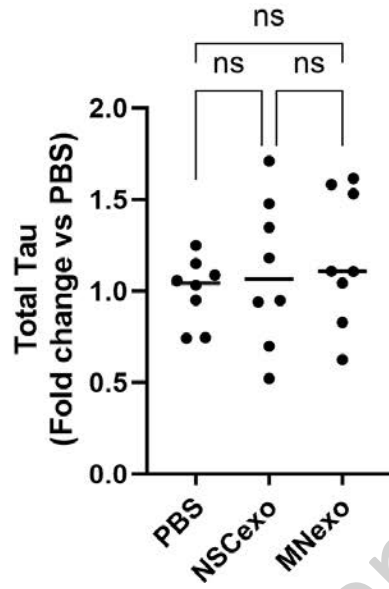
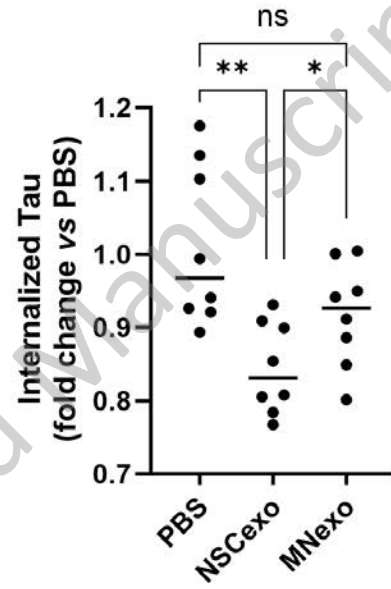




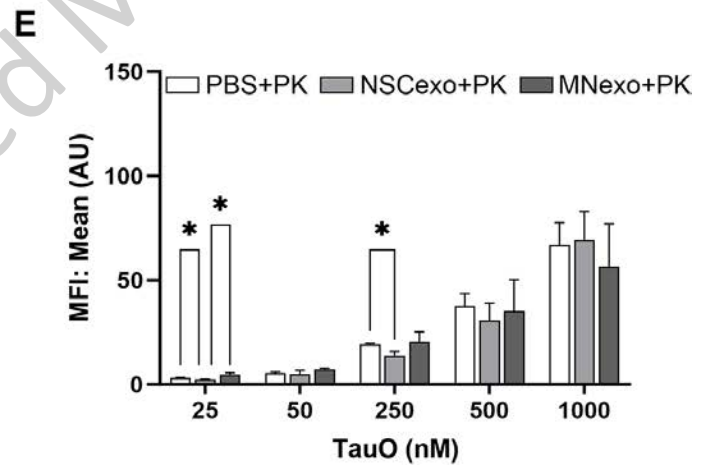
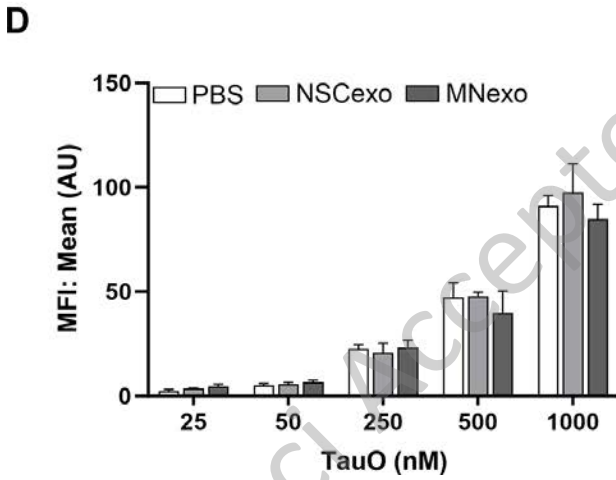
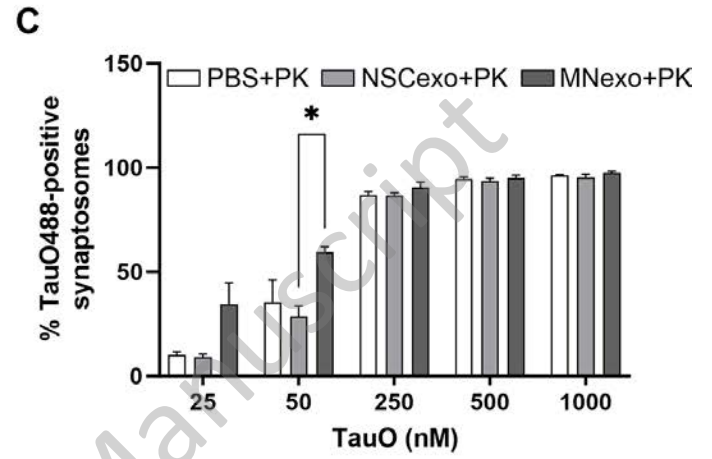
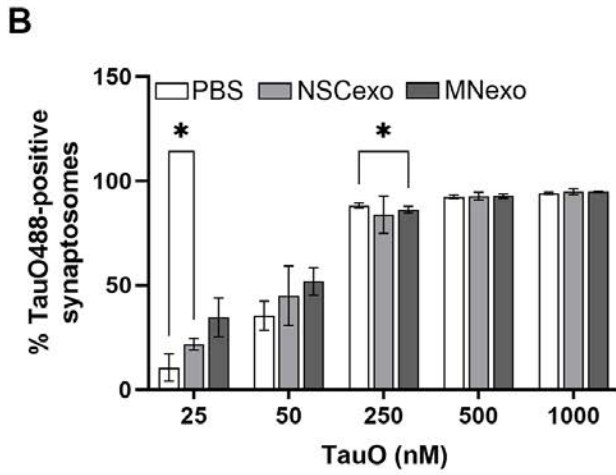
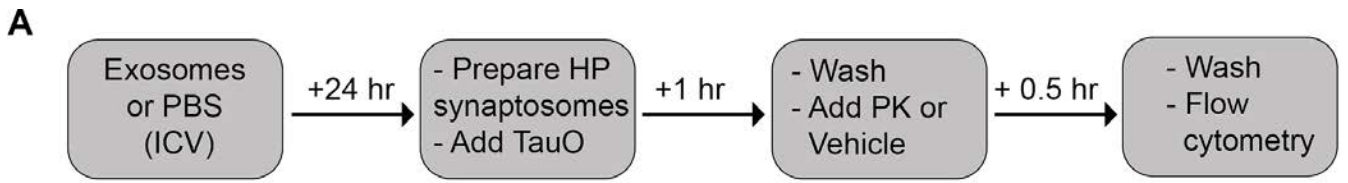
JNeurosci Accepted Manuscript



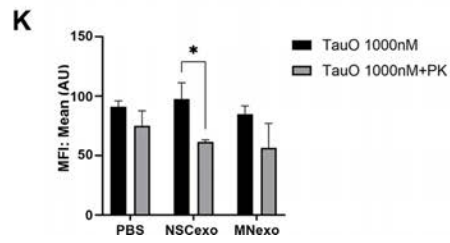
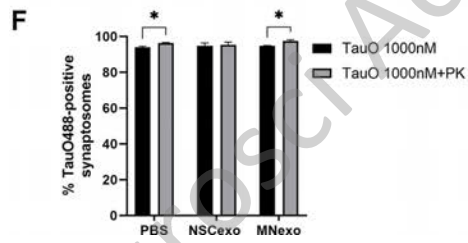
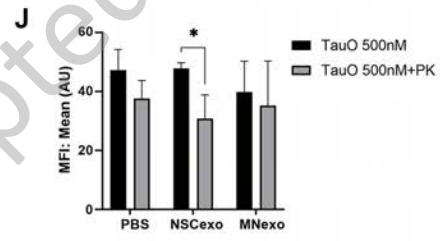
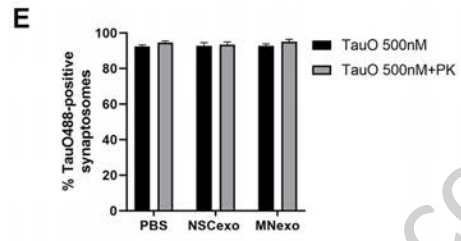
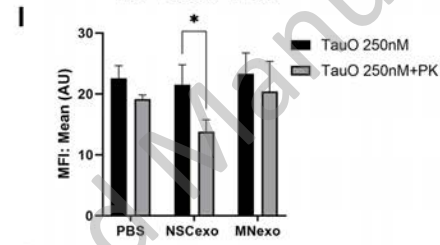
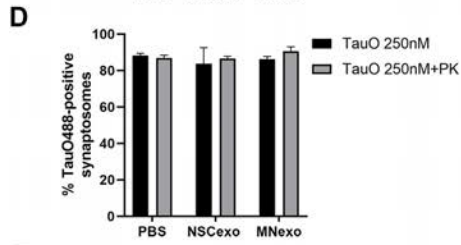
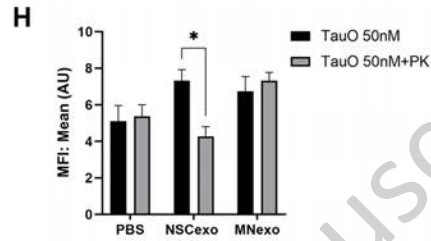
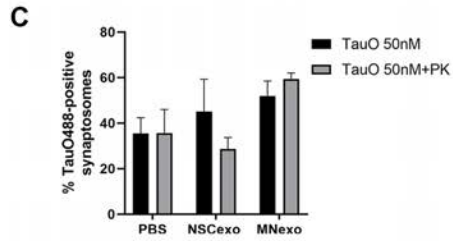
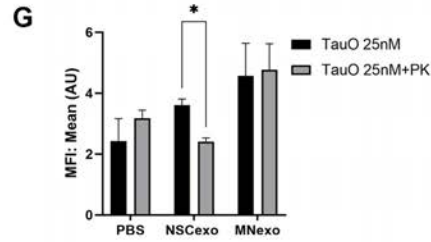
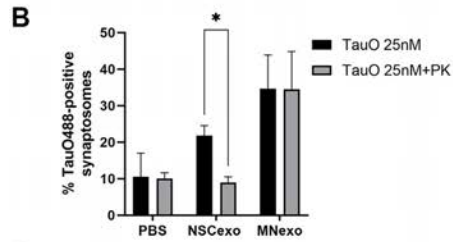
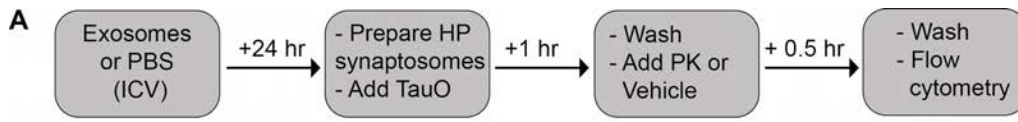
JNeurosci Accepted Manuscript

A**B****C**

JNeurosci Accepted Manuscript



JNeurosci Accepted Manuscript



JNeurosci Accepted Manuscript

